Universität Leipzig

Fakultät für Physik und Geowissenschaften

Felix-Bloch-Institut für Festkorperphysik

Abteilung Angewandte Quantensysteme

Investigation of GR1 Defect Formation in Single Crystal Electronic Grade Diamond under Oxygen Plasma Chamber Treatment

Bachelor Thesis

presented by:

Marvin Mellado Muñoz

Matriculation Number: 3741271

Primary Referee: Prof. Dr. Jan Meijer

Secondary Referee: Dr. Ralf Wunderlich

Leipzig, 28. Juli 2020

Contents

1 Introduction

Diamond is a material with many useful properties with regards to scientific and technological applications. In the Angewandte Quantensysteme research group at the Fakultät für Physik und Geowissenschaften, many of these applications are related to creating quantum systems for use in quantum computing, among others. Diamonds are found in nature but can be created artificially or enhanced via Chemical Vapor Deposition (CVD). These industrially produced and distributed diamonds, by companies such as Element Six, are relied upon for a number experiments [8].

The test originally carried out for this Bachelor's thesis was to corroborate measurements of GR1 color centers from previous studies. However, it was found that there were no such color centers and in fact a heavy amount of impurities (extrinsic defects) that were not expected. Further testing revealed extreme bleaching on the surface of our sample, which led us to conduct a plasma treatment for the following reasons. First, as a means to thoroughly clean up the sample, as much of the bleaching was suspected to be dirt that could not be removed with the other chemical procedures. Second, to test whether plasma chamber treatment of the sample creates any kinds of defects. The former is important due to the fact that removing dirt from the sample prevents nasty transients and unstable signals and allows us to take proper spectra from the sample. The latter is done partly as an exploratory test but also to test the findings of previous studies on the effects of plasma treatment [4]. The important point to consider is that if plasma treatment indeed causes defects such as the GR1 defect, then this could have implications for the future use these diamonds as instruments for quantum computing.

Indeed, GR1 defects were found after plasma treatment, along with other unexpected features. These defects where present under numerous levels of electron beam energy, as this beam is required to change the charge state of the GR1 vacancies and make them visible under Confocal Scanning Laser Microscopy. As a result this may provide an alternative method to create such defects when the advantages for quantum systems are desired. On the other hand it may be a cause for caution when such effects are not desired. In the following report, the experimental instruments, procedures and results of this research are described and discussed.

2 Theoretical basics

2.1 Classification of diamond

The generally accepted classification scheme for diamonds today is based on their macroscopic properties. It was proposed back in 1934 by Robertson et al [12]. Broadly speaking, most diamonds are Type I with nitrogen impurities and an absorption edge around 300 nm while the Type II remainder, devoid of nitrogen impurities have an absorption edge around 220 nm [12].

- **Type I:** Contains nitrogen impurities, typically 100-3000 ppm [8].

    - **Type Ia:** 95% of natural diamonds, contains aggregated nitrogen [8].
        * **Type IaA:** Contains nitrogen atoms in pairs.
        * **Type IaB:** Contains nitrogen atoms in large, even-numbered aggregates.
    - **Type Ib:** Contains single substitutional nitrogen [8].

- **Type II:** Very low nitrogen impurities, less than 5 ppm [8].

    - **Type IIa:** Corresponds to most CVD diamond, nitrogen is a major impurity [8].
    - **Type IIb:** Boron is the major impurity, can be p-type semi-conductors [8].

2.2 Color centers in diamond

Defects in the atomic structure (often referred to as color centers in the literature [2]), whether intrinsic or extrinsic, are responsible for the visible pigmentation in diamonds. The intrinsic defects can be caused by carbon atom vacancies, dislocated carbon planes or interstitial carbon atoms in the lattice. Extrinsic defects are impurities in the lattice, typically nitrogen, and can contain other elements. Natural diamonds usually have coloration, although coloration can also be created artificially. In general, coloration of diamonds depends not only on their internal defect (color center) content, but also on the type of radiation or particle beam used for observation [2]. By allowing the diamond to absorb particular energies of incident radiation, these defects give rise to spectroscopic features [11].

Below is a list of some of the crystallographic defects in diamond that are relevant to this study. Various features of uncertain origin are discussed later in the Results and discussion section.

- **GR1:** A defect with a pair of absorption lines at **740.9 nm** (1.673 eV)and at **744.4 nm** (1.665 eV) and associated bands. Thought to consist of a vacancy in a neutral charge state (V^0). Produced by natural or artificial irradiation [11].

- **NV$^-$:** An impurity and intrinsic defect with an absorption line at **637 nm** and associated bands. Thought to consist of a single substitutional nitrogen atom associated with a vacancy in a negative charge state (NV$^-$)[11].

2.2.1 The GR1 color center in diamond

The GR1 center (abbreviation of General Radiation) is an intrinsic defect that consists of an isolated vacancy in the diamond lattice in a neutral charge state. It has a Zero Phonon Line (wavelength at which no phonons are absorbed nor emitted) at 742 nm [10]. It can split into a doublet with lines at 740.9 nm and 744.4 nm [2].
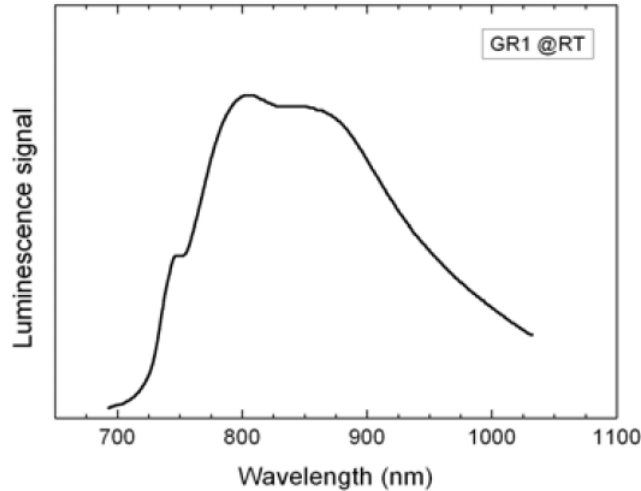

Figure 1: GR1 Photoluminescence spectrum measured in a natural, electron-irradiated diamond [10].

The GR1 center can be created in diamond by any irradiation including high-energy electrons, neutrons and ions [10]. The impurity content may affect the intensity of the center strongly. It may be suppressed or not appear at all in the following situations [2]:

- High nitrogen, neutron irradiated Type Ib diamonds.

- Highly boron doped Type IIb diamonds.

- After nitrogen implantation of sample.

- Hydrogen-terminated, ion-implanted, CVD diamond films.

The GR1 center can be observed with the following spectroscopic techniques [2]:

- Absorption spectroscopy

- Photoluminescence

- Cathodoluminescence

- X-ray excited luminescence

A low concentration of the GR1 center (below 5×10^{12} cm^{-3}) is always present in the top layer of CVD diamond films [2], such as that studied in this work.

2.3 Plasma treatment

Plasma, often described as the fourth state of matter, refers to a quasi-neutral collective of charged and neutral particles in a state similar to gas. For material processing, primarily low pressure plasmas are used. That is, plasma at pressures that are well below atmospheric pressure (usually <1000 Pa) [3]. In the experiments conducted for this bachelor's thesis, a pressure of 0.4 mbar was applied in all cases. For plasma generation a gas (such as O_2 in our case) must be ionized. The industrially most common method is based on electrical excitation [3]. An electrical voltage is applied to the plasma chamber filled with the process gas. Both AC and DC voltage or corresponding excitation frequencies are used for excitation. The available charging mechanisms are glow discharge, capacitive or inductive discharge. The electrons in the gas are accelerated due to this electrical energy, and have a large mean free path due to the low pressure. This can be approximately 10^{-3} m [4]. With sufficient kinetic energy, the electrons will impact and ionize the neutral gas particles, thus creating a plasma of positively charged ions and free electrons. This plasma is not in thermodynamic equilibrium, due to the fact that the electron temperature is much higher than the ionized gas temperature. This is called a nonthermal plasma. A sample inserted in such a plasma can be kept at room temperature and used for surface modification [13]. Different plasma compositions will create different potential applications, including etching, cleaning, depositing or increasing the reactivity of the surface of the sample. The exact composition of the plasma depends strongly on parameters such as the chemical composition of the gas, its fluency, pressure, reactor type, power, excitation frequency, chamber geometry and temperature. In order to estimate the surface effects of a plasma treatment, energy and particle-dependent surface processes are listed in Table 1 [3].

Plasma component	Kinetic Energy	Process	Depth
Ions, fast neutral particles	100 eV - 500 eV	Atomization, elastic collisions, implantation, defect creation	2 nm - 5 nm
	5 eV - 10 eV	Atomization from adsorbates, chemical reactions	monolayer
Electrons	5 eV - 10 eV	Inelastic collisions, Breaking of surface bonds, surface ionization	1 nm
Reactive, neutral particles	0.05 eV (thermal energy)	Adsorption, chemical surface reactions	Surface
Photons	>5 eV	Photochemical process	10 nm - 50 nm
	<5 eV	Secondary process	a few μm

Table 1: Possible surface effects of individual plasma components [3].

3   Experimental Methods

3.1   Confocal Scanning Laser Microscope

For the optical detection of GR1 centers the photoluminescent electronic transitions must be stimulated. The design of the confocal laser scanning microscope (CLSM) offers a high spatial resolution in the excitation of the sample as well as the detection of the emitted radiation. The layout of this instrument, or rather, ensemble of instruments, is shown schematically in Fig. 2. For excitation, several lasers were attempted with varying results in the quality of the fluorescence for the purpose of finding color centers. These include:

- 593 nm (orange) (w/ 593 notch, 593 LP filter)

- 532 nm (green) (w/ 532 notch, 550 LP filter)

- 488 nm (blue) (w/ 488 notch, LP filter)
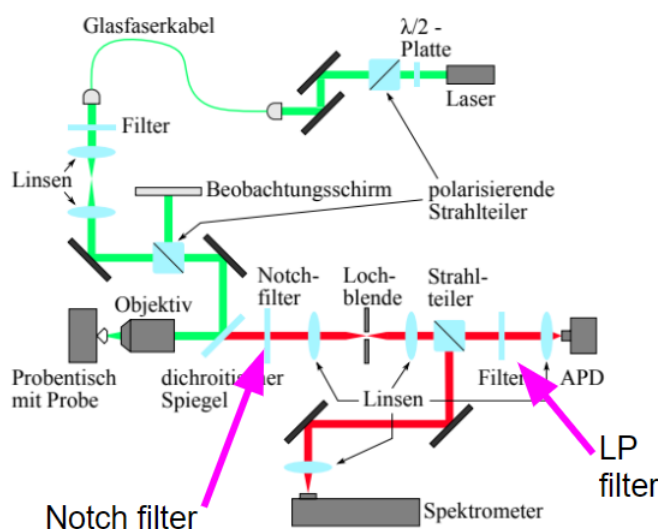
Figure 2: Simplified Schematic of the Confocal Laser Scanning Microscope [6].

The laser beam is maximally focused by a lens system, so that the excitation occurs in the smallest possible volume range. A pinhole, which is installed in front of the detector ("Lochblende" in Fig. 2) allows for depth resolution. This aperture allows only light rays emitted by the sample to pass from a certain depth. The volume area excited by the laser and that transmitted through the pinhole depth level are the two factors that contribute to the local resolution. This allows a lateral resolution of 300 nm (air objective) and an axial resolution of 1 μm (air objective). The smallest possible excitation volume is 0.023 μm^3 [4].

It's necessary to obtain a spectrum of the sample in order to find the spectroscopic features, in addition to raster scans of the sample surface to locate irradiated areas or areas of interest, and to observe possible bleaching effects. Therefore, our data will appear in the form of spectra and 2D fluorescence images. For detection, the following instruments are used:

- HORIBA Jobin Yvon Spectrometer

- Two Perkin Elmer Avalanche Photodiodes (SPCM-AQRH 14)

These instruments are indicated in Fig. 2 as "Spektrometer" and "APD" respectively. The spectrometer has a spectral range of 400 - 1060 nm, and in all cases the spectra were captured with a shutter time of 1 s with a total of 200 accumulations and a count frequency of 200 Hz. The photodiode used is a Single Photon Counting Module (SPCM) made of silicon from the manufacturer Perkin Elmer with the Designation SPCM-AQRH 14 [14]. The avalanche photodiode exploits the photoelectric effect to convert light into electricity, like a photomultiplier. The detection efficiency indicated by the manufacturer is wavelength-dependent, but is no more than 65% at a wavelength of 650 nm [14]. The associated software can use the photodiode to take raster scans of the sample. This is done with piezoelectric screening units which can be manually adjusted or commanded from the software.

3.2 Electron Implantation

The Nova NanoLab 200 Electron Microscope was used and operated by Dr. José Barzola Quiquia. The purpose was to irradiate the diamond sample with a set of $50 \times 50 \mu m$ electron irradiation zones. All implantations were done with a fluency of 5500 $\frac{\mu As}{cm^2}$. These zones would each have different electron beam energy, generally with discrete increments from 1 keV up to 30 keV. These electrons would later provide visible fluorescence in the Confocal Scanning Laser Microscope and potentially reveal the GR1 spectroscopic features, among others. Figures 3 and 4 show the electron microscope and where the sample was inserted. Dr. Barzola Quiquia navigated across the sample's surface using the viewport, as shown in Fig. 5. The viewport images were generated with live secondary electron from the low power scanning mode of the electron microscope, however the implantations themselves involved applying the beam for longer duration (typically a couple of minutes for a single implantation zone).
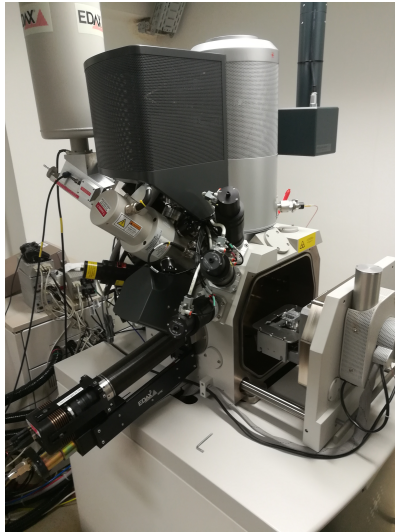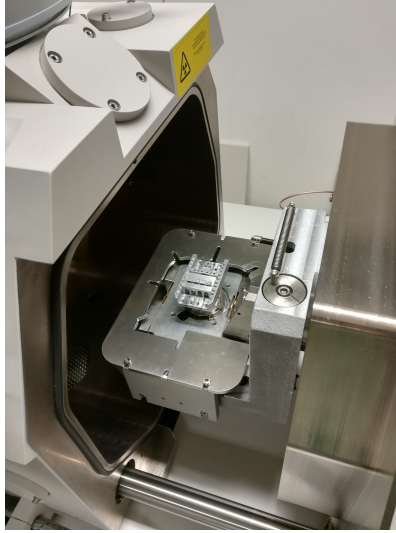

Figure 3: Electron Microscope.

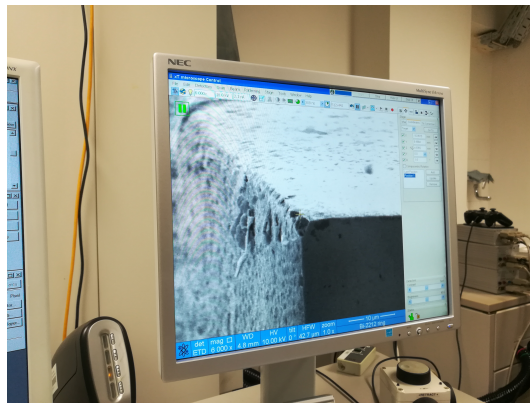Figure 4: Close-up of the Electron Microscope sample holder.

Figure 5: Observing a corner of the sample with live secondary electron emission via the Electron Microscope software viewport.

3.3 The Sputter Coater

The Cressington Sputter Coater was used to coat the diamond sample with 160 nm of gold in preparation for the plasma treatment. As will be illustrated later in the sample preparation section, the goal of the gold layer is to prevent ion implantation in the plasma chamber onto the sample everywhere except where the gold will be scratched off. The sputter coater itself is shown in Fig. 6. The sample is placed in a vacuum chamber on a rotating plate, which serves as an anode. Above the sample are two high-purity targets made of the metal of choice (gold, in this case). These targets are the cathodes. Argon gas is introduced into the chamber and ionized, forming a plasma. This plasma is composed of Argon cations and electrons. If a voltage is applied, Argon ions are accelerated to the targets and knock out some of its atoms. These knocked out atoms fall upon the sample, thus creating the desired layer over time [5].
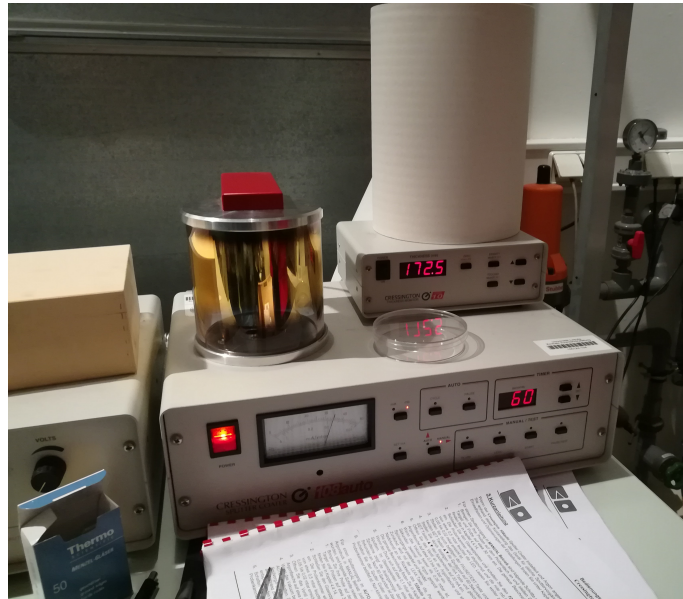
Figure 6: Sputtercoater

3.4 Plasma Chamber

The plasma system used here is the model "Pico" of the company "Diener electronic", as shown in Fig. 7. This is a low-pressure plasma system that uses the plasma generated by AC voltage. Fig. 8 shows the schematic structure. The two electrodes are arranged around the cylindrical vacuum chamber made of quartz glass. Around the glass cylinder two electrodes are arranged, which are connected to a high frequency generator. The desired gas is fed into the cylinder and the generator generates a plasma by capacitive-electrical excitation. The cylinder of the system has a volume of 5 liters and the high-frequency generator delivers a frequency of 40 kHz. The maximum achievable power is 200 W [5]. A flat sample carrier of Quartz glass is located in the middle of the plasma chamber and is electrically decoupled. As a result, a sample is exposed to only low ion bombardment, since corresponding ion energies at electrically decoupled sample holders are comparatively small (<10 eV) [4]. The discharge at 40 kHz is given by the plasma ion frequency,

$$\omega_i = \sqrt{\frac{e^2 n_0}{\epsilon_0 m_i}}$$

Where n_0 is the ion density and m_i is the ion mass so that the ions can follow the alternating electric field and secondary electron emission on the cathode wall. A plasma with ionization densities of about $10^{10} cm^{-3}$ forms between the electrodes [3]. This set-up generates a large homogeneous plasma distribution around the sample, so that an isotropic process is present [4].

According to the manufacturer, this plasma treatment is primarily suitable for cleaning by removing organic layers [7]. Here is a summary of the parameters used in this study:

- O2 Gas

- Pressure: 0.4 mbar

- Room temperature (temperature rose to a maximum of 63°C during experiment)

- Maximum power (200 W)

- AC Voltage frequency of 40 kHz

- Glow discharge

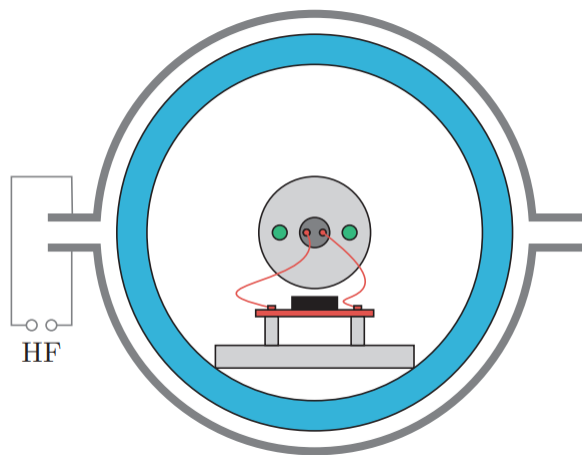Figure 7: Plasma Chamber from the "Diener electronic" company.

Figure 8: Plasma Chamber schematic, cylindrical cross-section [5].

3.5 Sample preparation

3.5.1 Diamond sample

The diamond sample used for the present work is a single crystal "Electronic Grade Diamond" produced by Element Six. It's characterized by high crystalline purity, with Nitrogen impurities at <5 ppb and Boron impurities at <1 ppb. However, the high quantity of NV centers found in the initial observations indicate that this specific asset may not have been quite up to the standard. The sample was grown by chemical vapor deposition and is classified as a Type IIa diamond. This sample came with the dimensions of $2 \times 2 \times 0.5$ mm. The surface corresponds to the crystallographic {100} plane in the diamond and is specified by the manufacturer with an error up to $3°$. The datasheet of this sample is included in the appendix in Fig. 50 and was obtained from the manufacturer's website [8]. Fig. 9 shows the case and serial number the sample came with.

Figure 9: Diamond Sample case and label.

3.5.2 Preparation sequence

Before initial observations with the Confocal Scanning Laser Microscope, the sample was subjected to a cleaning procedure to prevent dirt from causing undesired artifacts in the measurements. Ethanol was sprayed on Kimtech lab wipes and the sample was carefully rubbed against the dampened surface. The use of tweezers is necessary due to the tiny cross section of the sample. It was then left in a mixture of ethanol and acetone overnight. Once ready, it was glued to a silicone wafer with Leitsilber G302. With a small circular sticker, it's placed on a relatively large sample holder which is then inserted into the optical lattice of the Confocal Laser Scanning Microscope.

Due to the fact that the effects of the plasma chamber upon the fluorecence spectra were uncertain, it was taken as a precaution to first create a 160 nm layer of gold on the sample. The idea was to then scratch out a window where the electron implantations would take place, and subsequently isolate the rest of the sample from the plasma treatment. That way, it was possible to test for different durations of plasma treatment on the same sample. As for the scratching of the windows, it was done with the combination of a standard optical microscope and a pair of mechanically controlled scratching probes, seen in Fig. 11. This process had to be done carefully, with one probe holding the sample down and the other removing the gold with restricted movement. A rectangular area had to be cleared with enough room for all necessary electron implantations meant for a given plasma treatment.

Fig. 10 shows how the sample is split up into experimental sections. Below is a list of the experimental steps as they are labeled in the Results and Discussion section.

- Plasma Treatment 0 (no plasma)

- Plasma Treatment 1 (45 minutes in plasma chamber)

- Plasma Treatment 2 (20 minutes in plasma chamber)

It's important to note that the 90 minutes plasma treatment data was omitted from this study due to suspected hydrogen gas contamination (as no useful spectra were actually visible). However, its location is still displayed in the diagram of Fig. 10.
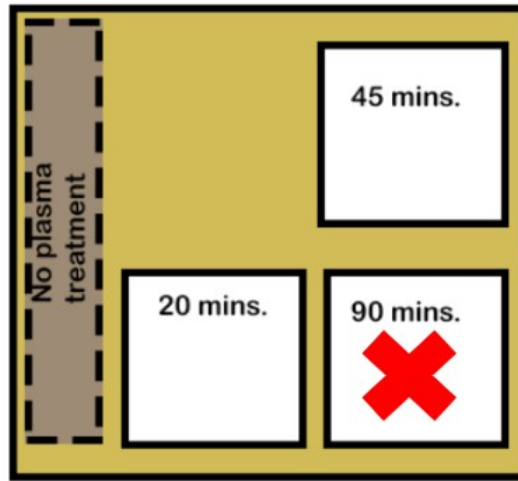
Figure 10: Diamond Sample areas of irradiation and experimental steps.
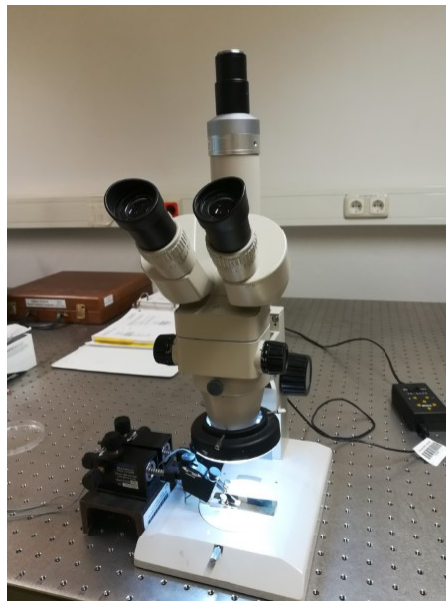
Figure 11: Optical microscope with mechanically controlled "scratching" probes.

4 Results and discussion

4.1 Reference measurements before implantation

4.1.1 Overview

Before performing any modifications to the sample, it was first cleaned up and left in an ethanol-acetone solution for a night. It was then measured directly with CSLM. The first attempted configuration was with the 532 nm (green) laser, utilizing 532 notch and 550 LP filters. An area of 600 × 600 μm was scanned. A laser power of 840 μW. Many NV centers were observed in the sample, up to 20 in a random 20 × 20 μm area, which can be clearly seen in Fig. 12. This was contrary to our expectation based on the manufacturer's parameters regarding purity [8].

A spectrum was taken at the NV center at the coordinates (46.6, 3010) μm, along with a corresponding background which is subtracted. It's plotted in Fig. 13. It was captured with a shutter time of 1 s with a total of 200 accumulations and a count frequency of 200 Hz. As expected, no GR1 signal was visible. One interesting feature that appeared is a peak at 597 nm which appears to be a cosmic event. Other than that there is the NV$^-$ ZPL at 637 nm and its corresponding sideband.

4.1.2 APD images
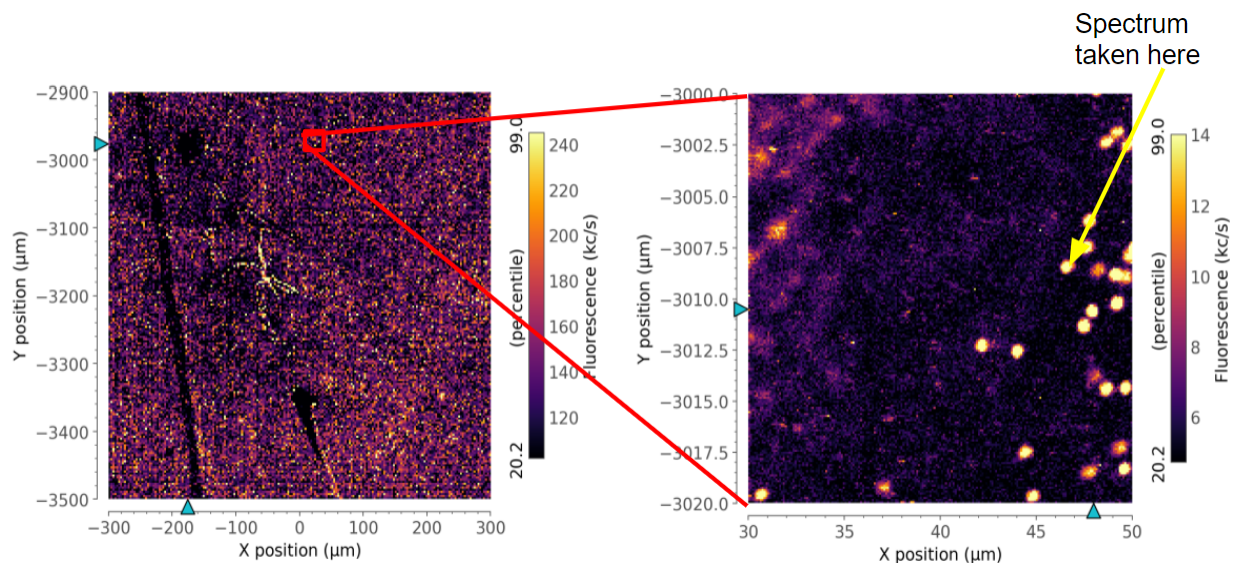
Figure 12: APD Image of the sample before any electron implantation.

4.1.3 Spectrum
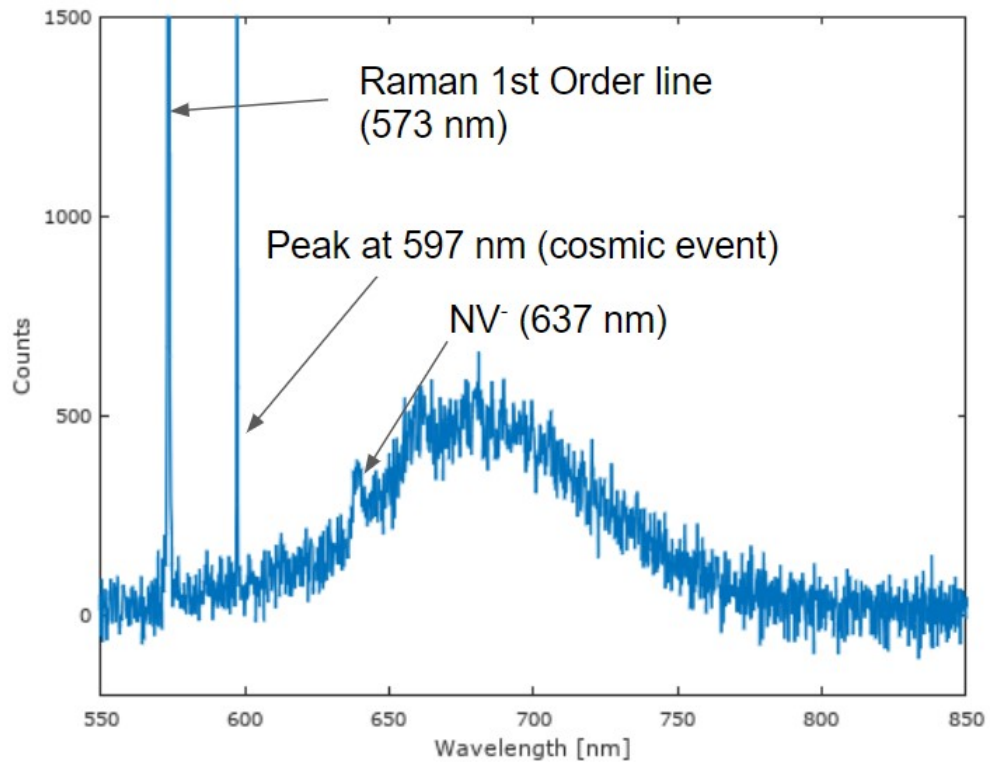
Figure 13: Background-subtracted spectrum of the sample before any electron implantation. Raman first order line, NV⁻ Zero Phonon Line and a likely cosmic event are indicated.

4.2 Plasma treatment 0 (no plasma)

4.2.1 Overview

The first electron implantation was conducted on one column on the left hand side of sample. It consists of seven $50{\times}50\mu$m implantation zones with varying implantation energy, but all with an equal fluency of 5500 $\frac{\mu As}{cm^2}$. An additional 10 keV "Test" zone of $100{\times}100\mu$m was added in order to test methods and calibrate equipment. No plasma treatment was performed at this stage.

CLSM measurements were taken directly after electron implantation. The orange laser ($\lambda =$ 594 nm, power = 53 μW) was used along with a 594 notch and 594 LP filters. An overview of all irradiations can be seen in Fig. 14, with an APD image and a diagram showing exact coordinates. Bleaching tests were conducted for most of the implantation zones, shown from Figs. 15 to 18. Bleaching corresponds to a permanent loss of the charge state in a given region of the sample due to prolonged exposure to the laser. This causes a significant reduction in the fluorescence photon counts. Significant bleaching prevents the acquisition of reliable spectra from the region in question. In these tests even one raster scan was enough to create visible signs of bleaching. For each irradiation zone there are three images, one to show how it looks before bleaching, a second in which a corner is bleached and finally a third in which the bleaching effect is plainly visible. Fluorescence in the sample was not at all stable and the laser was able to quickly burn "holes" in the fluorescence of the sample.
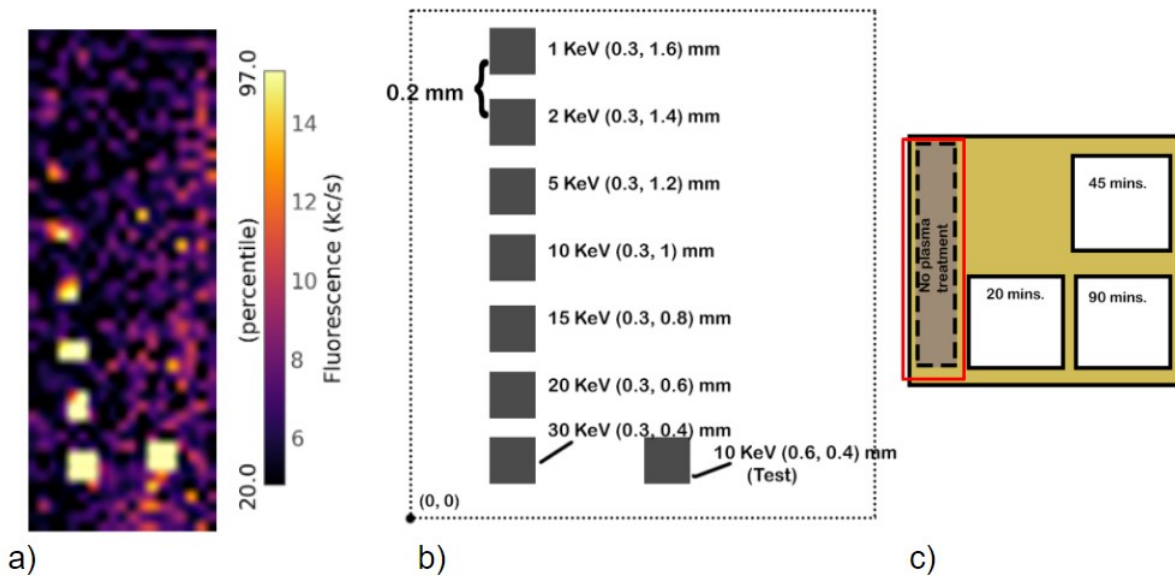
Figure 14: a): APD Image of all six implantation zones after 1st plasma treatment. b): Diagram with coordinates of implantation zones relative to sample origin. c) Location of this experimental step relative to the others in the study, highlighted in red.
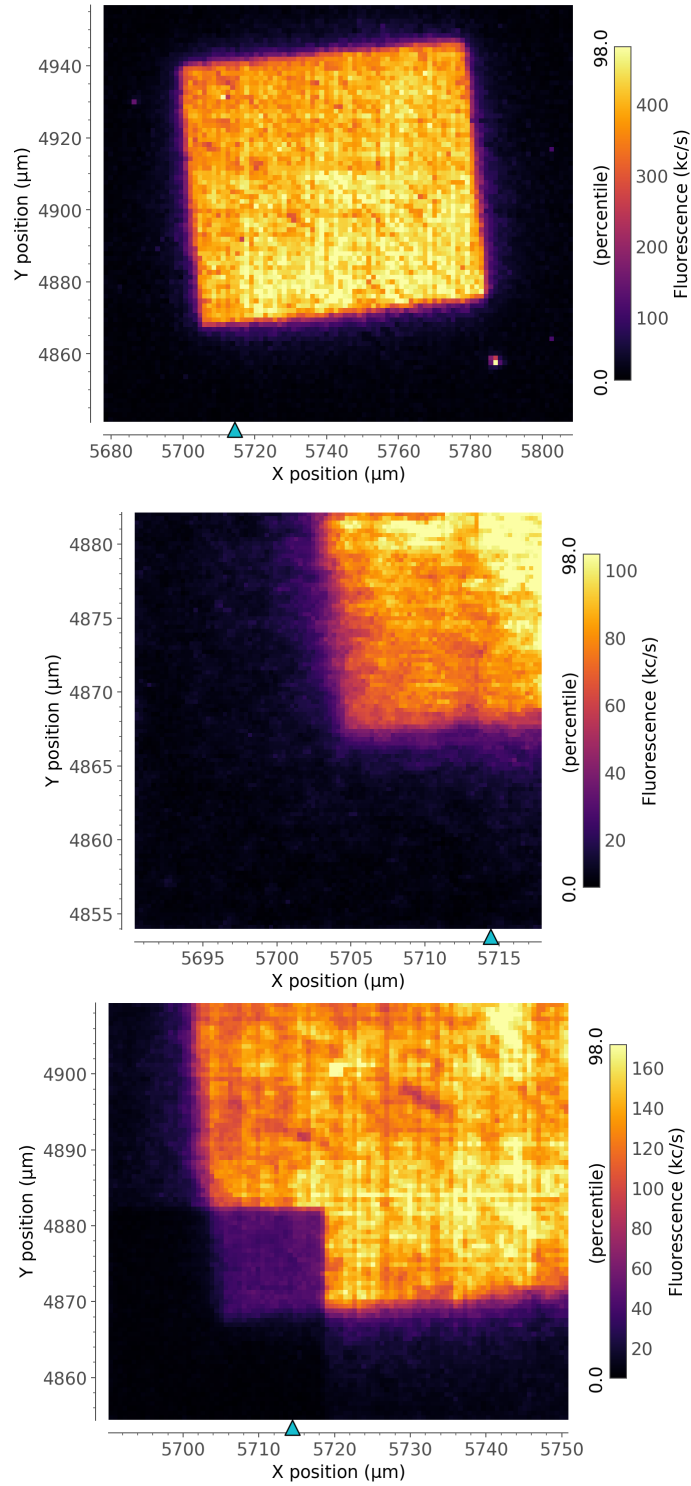
Figure 15: APD Image of 10 keV zone without any plasma treatment. Top: before bleach. Middle: inset bleach. Bottom: after bleach
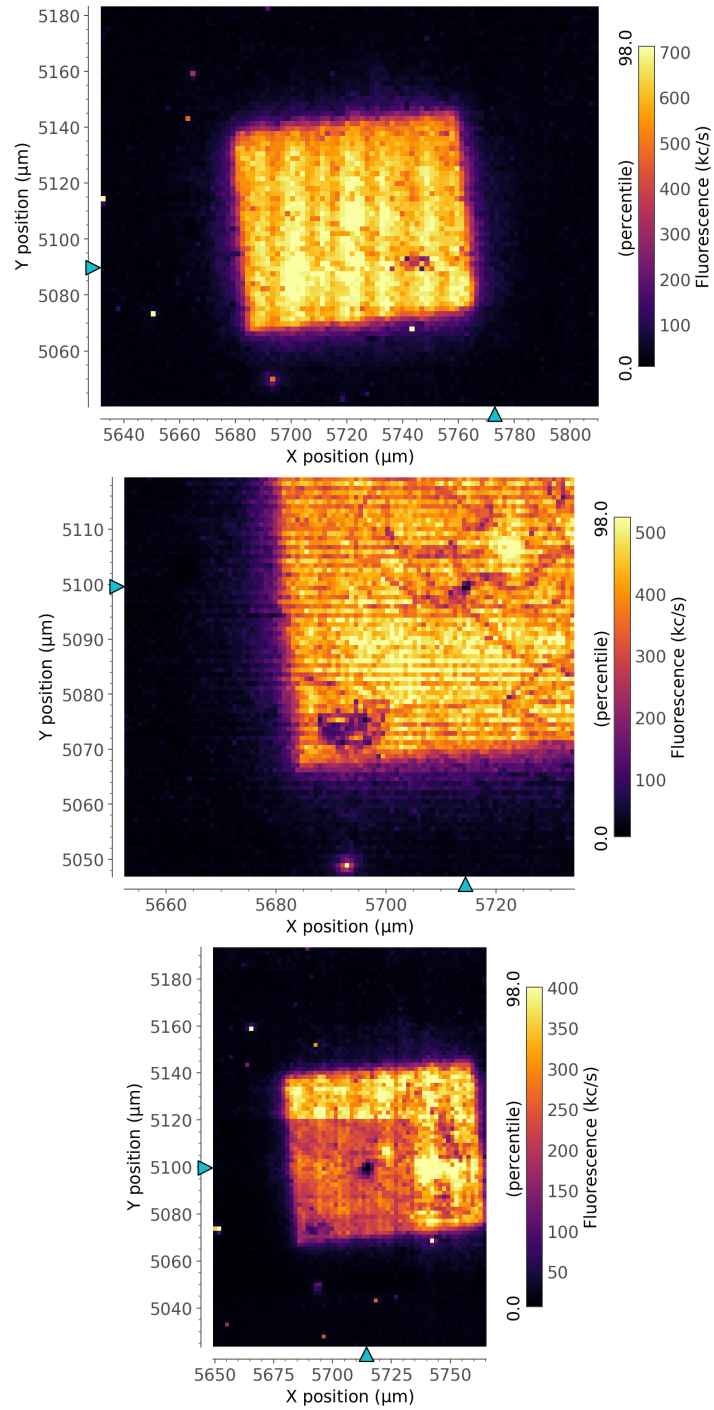
4.2.3 15 keV

Figure 16: APD Image of 15 keV zone without any plasma treatment. Top: before bleach. Middle: inset bleach. Bottom: after bleach
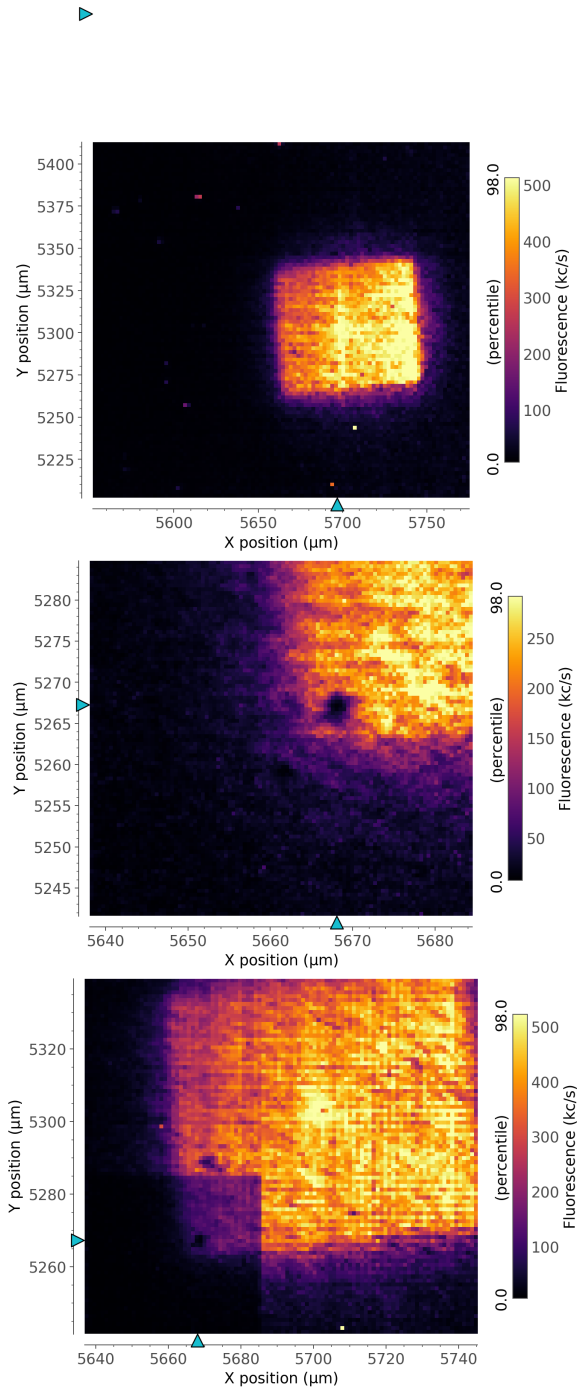
4.2.4 20 keV

Figure 17: APD Image of 20 keV zone without any plasma treatment. Top: before bleach. Middle: inset bleach. Bottom: after bleach
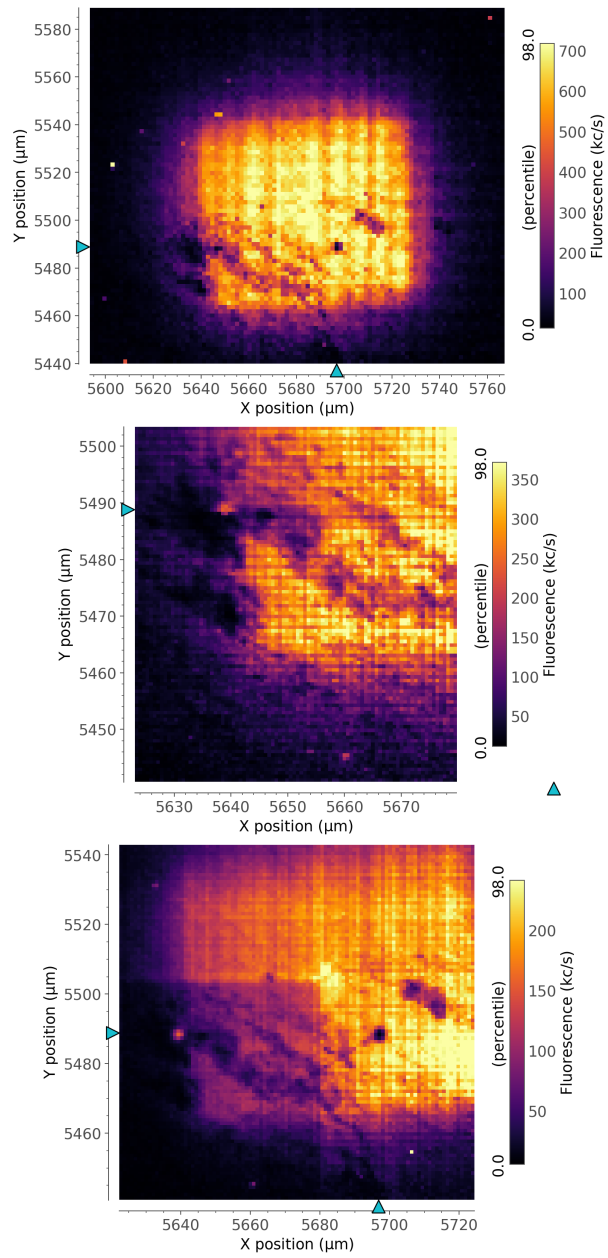
4.2.5   30 keV

Figure 18: APD Image of 30 keV zone without any plasma treatment. Top: before bleach. Middle: inset bleach. Bottom: after bleach

4.2.6 Spectrum

For capturing the fluorescence spectrum of the sample, a blue laser ($\lambda = 488$ nm) was used on the 15 keV implantation zone. It was captured with a shutter time of 1 s with a total of 200 accumulations and a count frequency of 200 Hz. No GR1 features were detected (Fig. 19), only a peak at 524 nm, presumably a cosmic event. Fig. 20 shows the location where the spectrum was taken. Unfortunately, at the time these measurements were taken, the research was in an exploratory phase and a more systematic measuring process hadn't been applied yet. As such, the opportunity was lost to record measurements with other lasers and perform background measurements, due to the fact that the sample surface would be altered. As such, only the raw data is available in this instance.
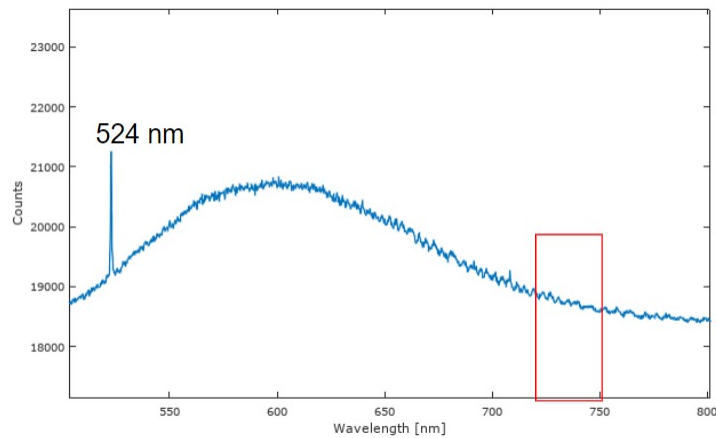
Figure 19: Spectrum of the 15 keV zone. Highlighted in red is where we expected to see a GR1 feature, but found none. In addition, a likely cosmic event at 524 nm.
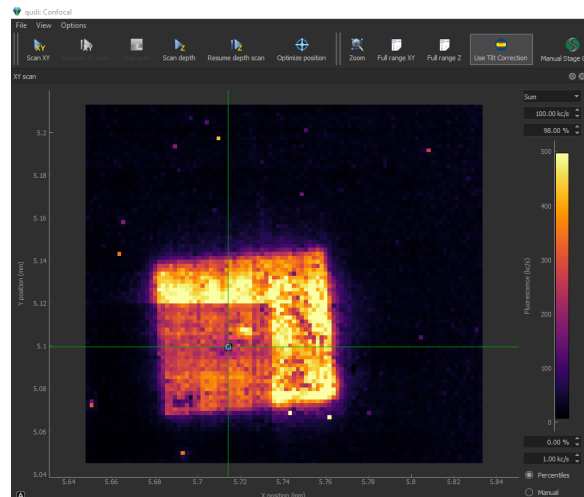
Figure 20: Location within the 15 keV zone where the spectrum was taken.

4.3 Plasma treatment 1, 45 minutes

4.3.1 Overview

Due to extreme bleaching on the sample it was decided to oxigenate the sample via plasma treatment and measure again. In preparation for multiple plasma treatments the sample was first coated with 160 nm of gold with the Sputter Coater. Then, small windows (less than a quarter of the sample surface) were to be scraped off with the microscope-probe configuration previously discussed. That way, the plasma chamber would only affect one intended area at a time. In this section, the results for a plasma treatment of 45 minutes, with O_2 gas, 0.4 mbar pressure and room temperature are illustrated. Fig. 21 shows all the implantation zones, a diagram of their relative locations and corresponding implantation energies, and the relative location on the sample. We measured 4 spectra for each of the six implantation zones with the orange laser ($\lambda = 594$nm, power: 3.8 mW), which are as follows:

- Point measurement inside the implantation zone

- Point measurement outside the implantation zone (background)

- Area measurement inside the implantation zone (10×10 μm)

- Area measurement outside the implantation zone (background) (10×10 μm)

All spectra have their corresponding background subtracted. In all cases the spectra were captured with a shutter time of 1 s with a total of 200 accumulations and a count frequency of 200 Hz. There is an unknown feature that shows up at 673 nm that stands out. It appears with varying intensity. It does not correspond to the typical features that are expected of this diamond, however potential candidates are discussed later.

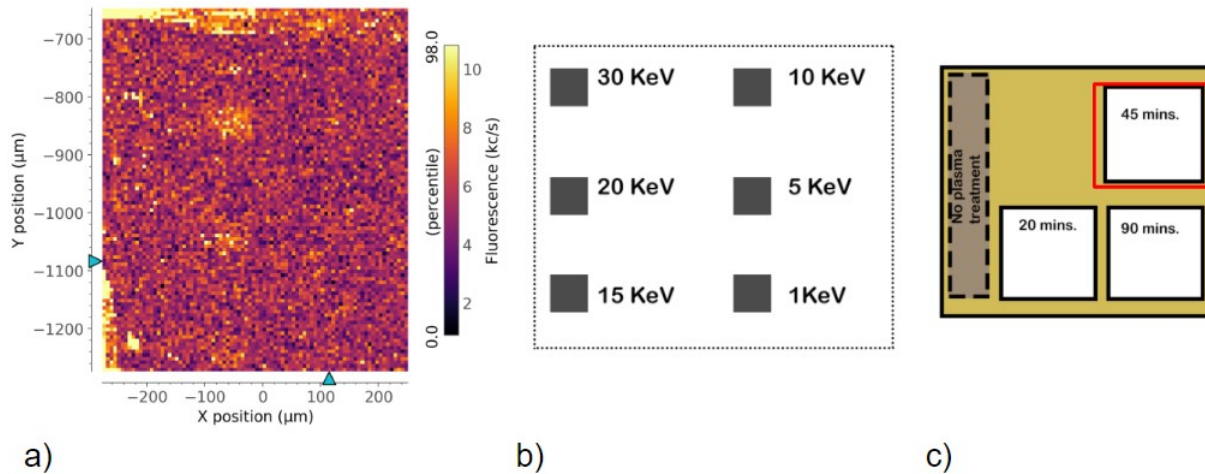a)   b)   c)

Figure 21: a): APD Image of all six implantation zones after 1st plasma treatment. b): Diagram of all six implantation zones after 1st plasma treatment. c): Relative location on the sample of this experimental step.

4.3.2 1 keV

In this section the APD images and spectra corresponding to the 1 keV implantation zone (first plasma treatment) are shown.
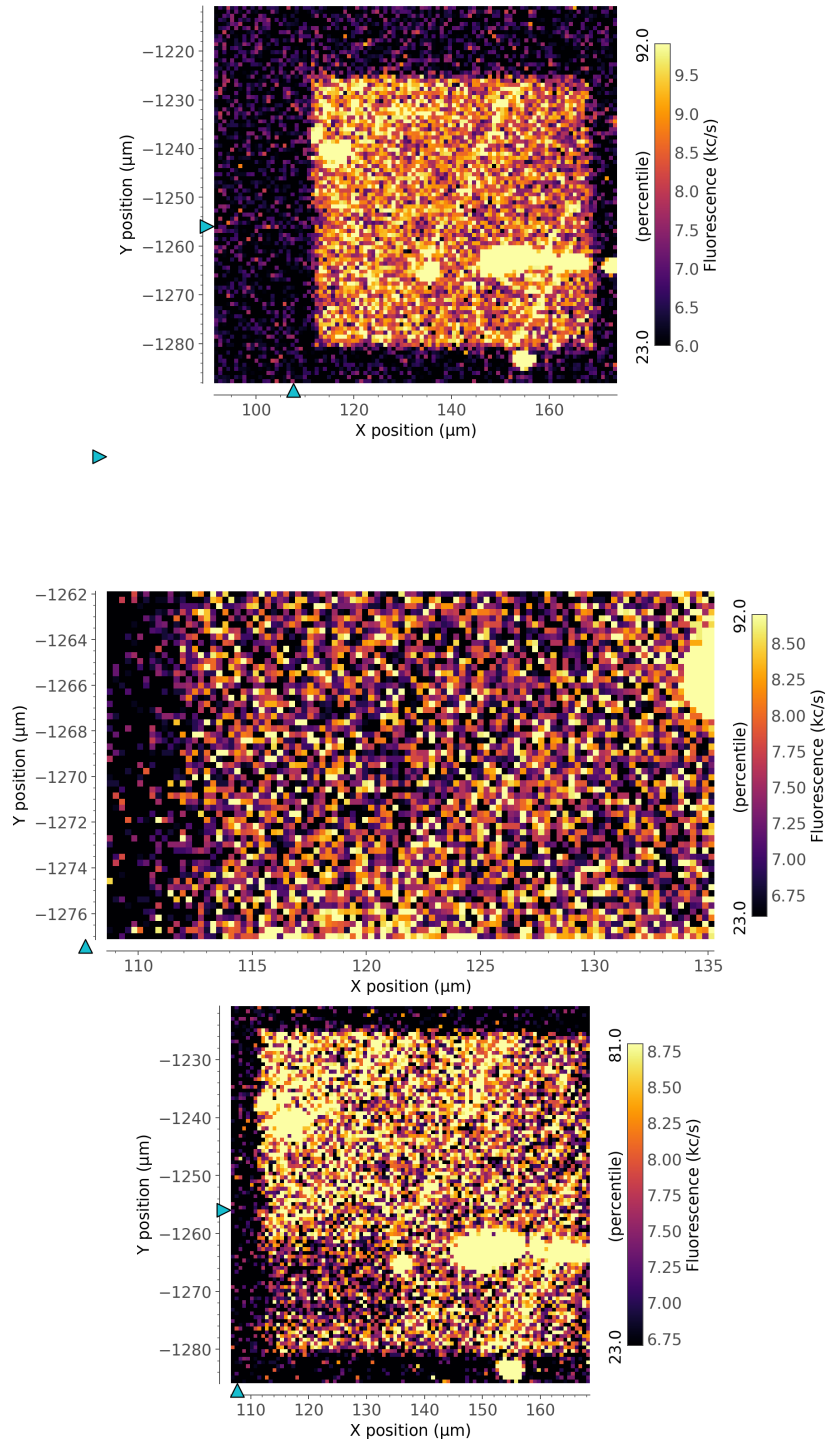

Figure 22: APD Image of 1 keV zone after 1st plasma treatment. Top: before bleach. Middle: inset bleach. Bottom: after bleach
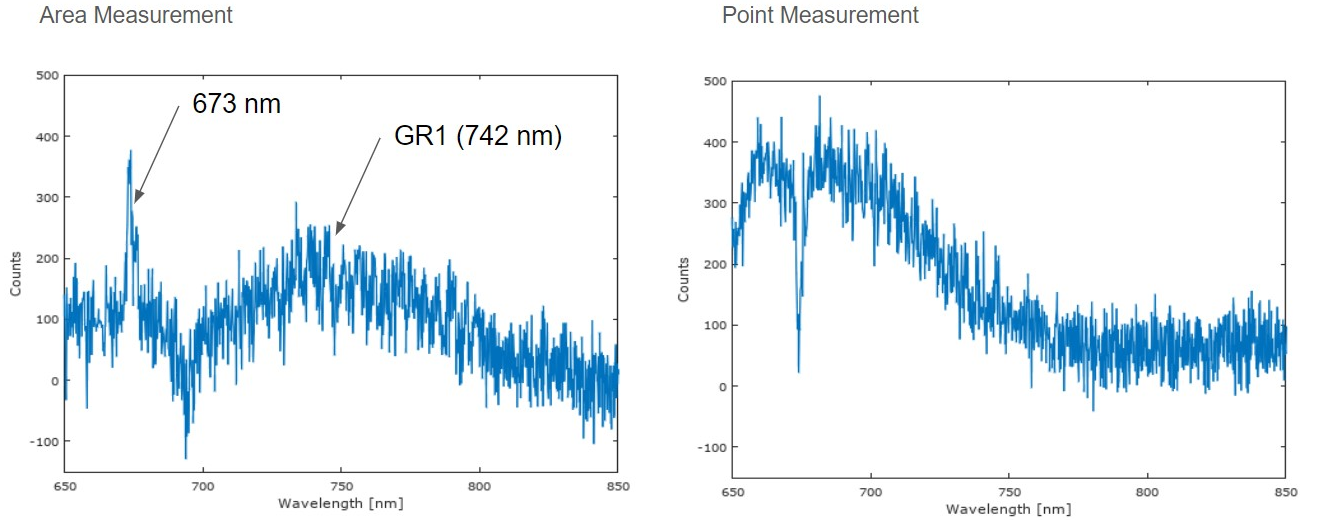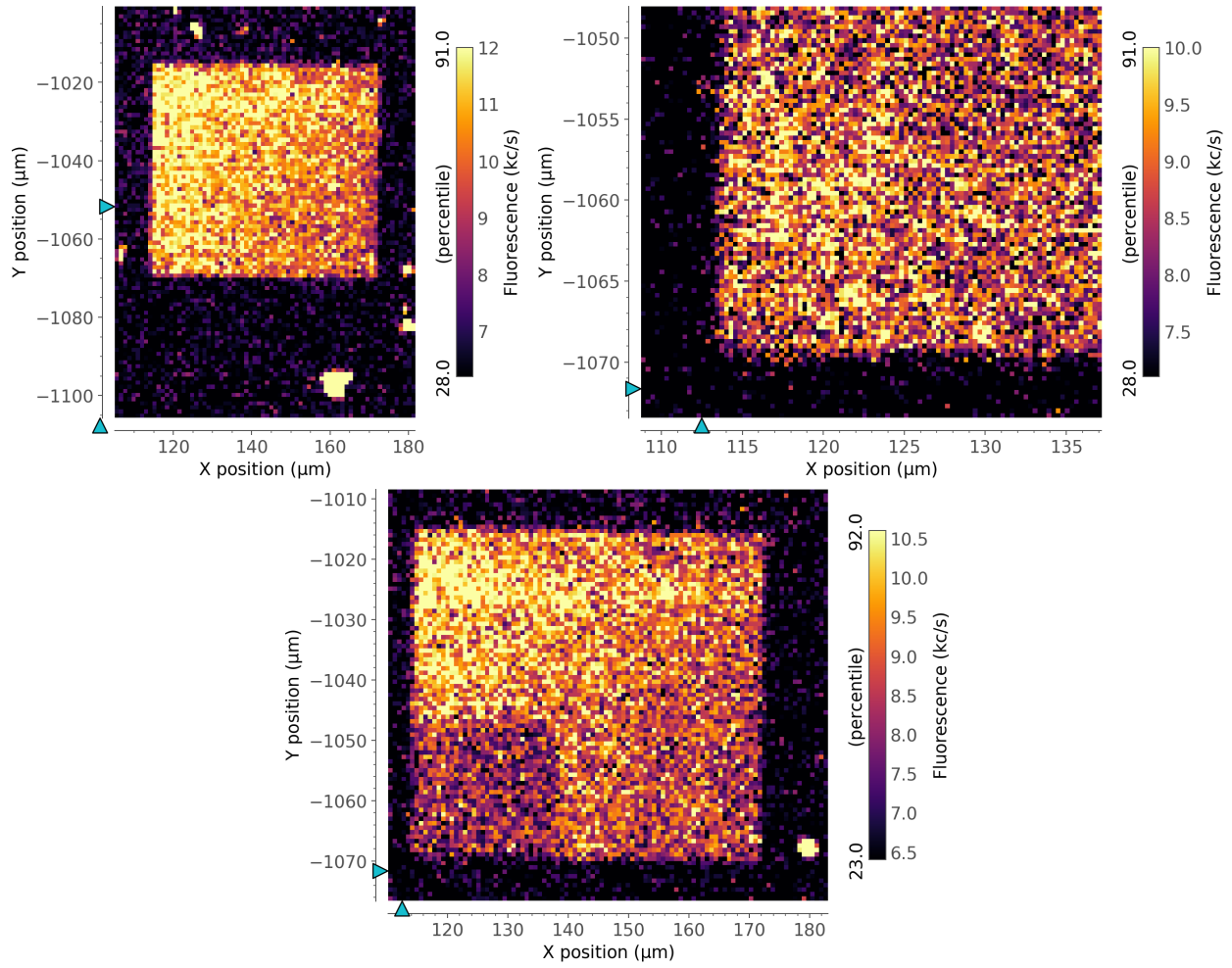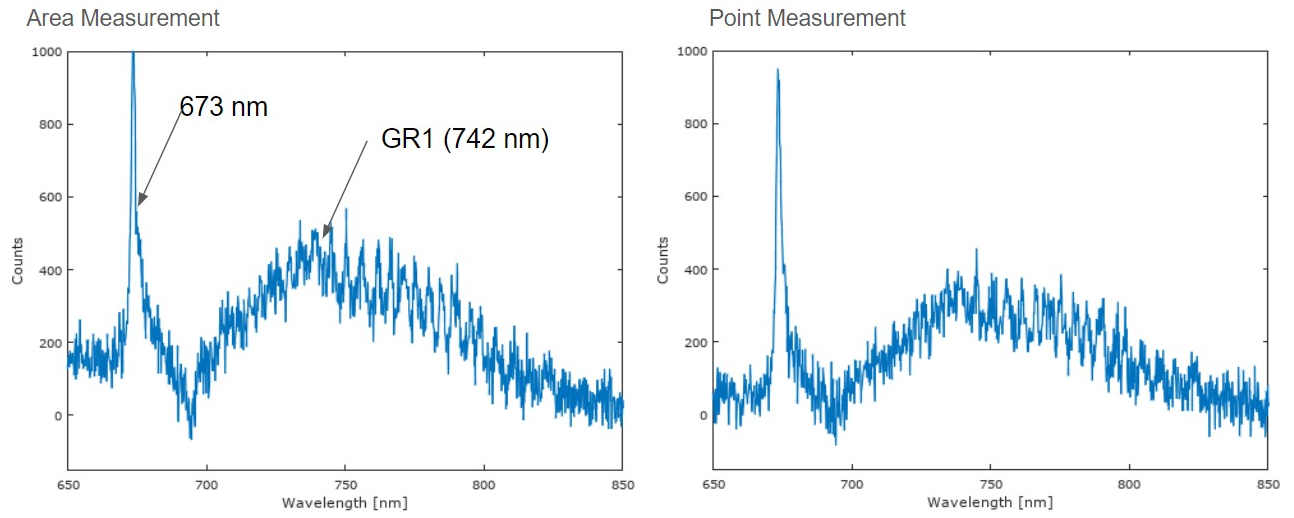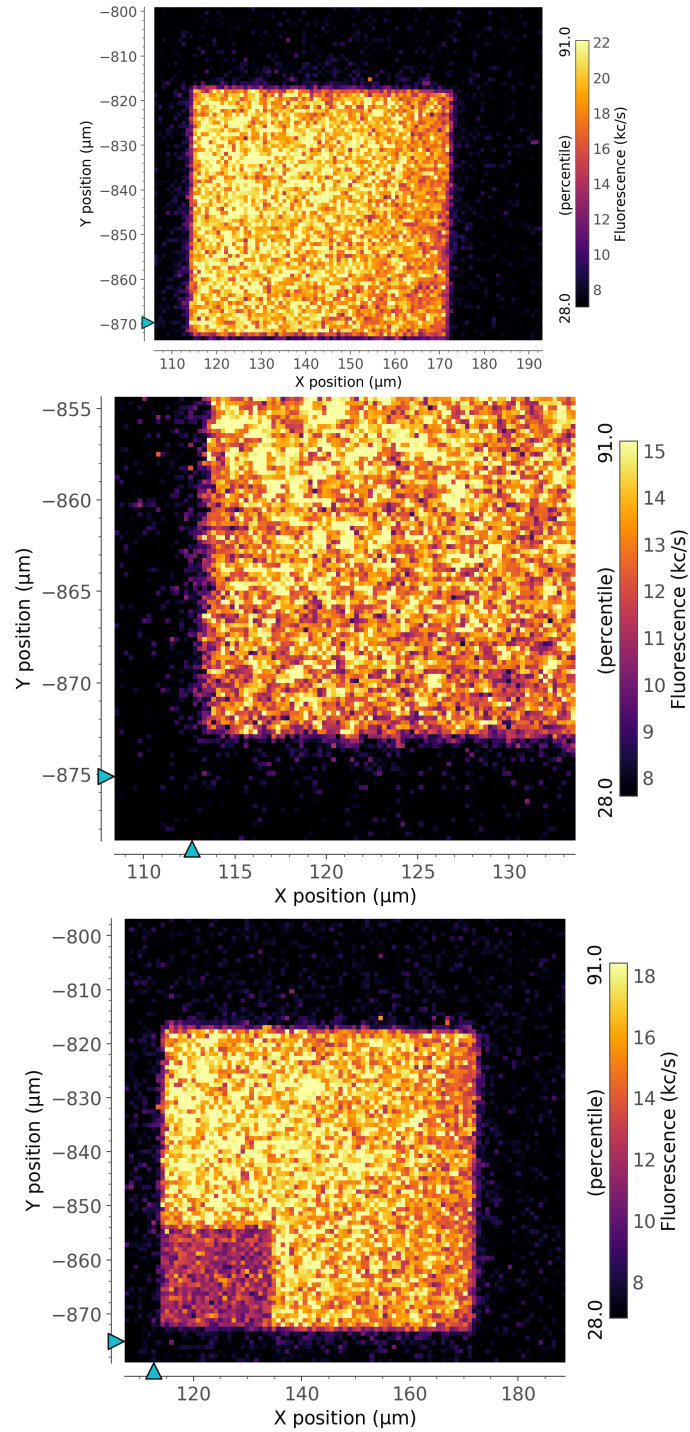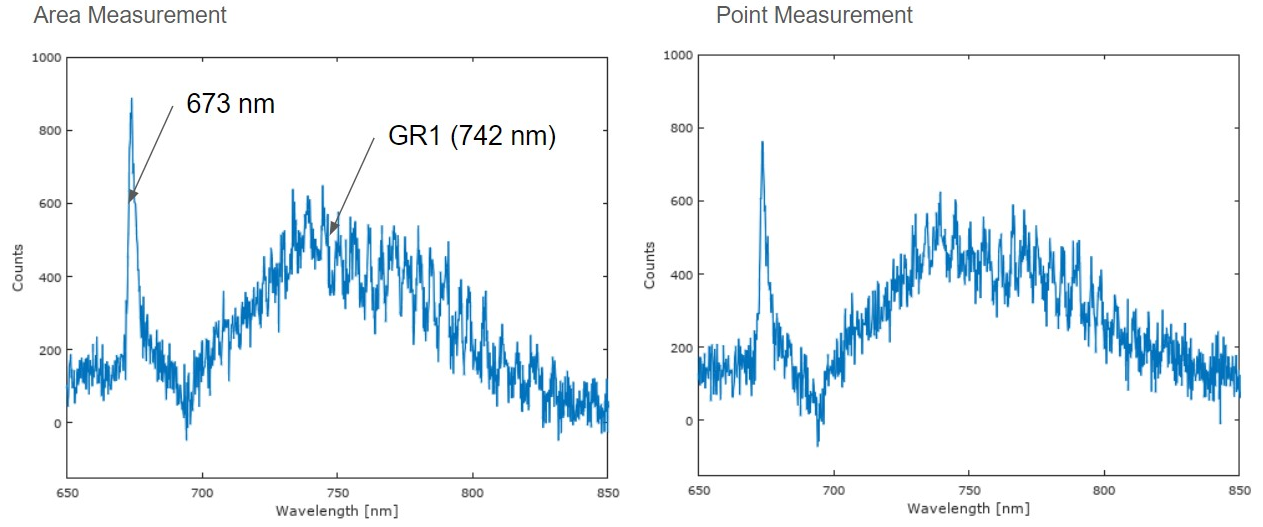
Figure 23: Spectra of the 1 keV zone after 1st plasma treatment. GR1 ZPL and an additional feature are indicated. Left: Area measurement. Right: Point measurement.

4.3.3   5 keV

In this section the APD images and spectra corresponding to the 5 keV implantation zone (first plasma treatment) are shown.

Figure 24: APD Image of 5 keV zone after 1st plasma treatment. Top left: before bleach. Top right: inset bleach. Bottom: after bleach

Figure 25: Spectra of the 5 keV zone after 1st plasma treatment. GR1 ZPL and an additional feature are indicated. Left: Area measurement. Right: Point measurement.

4.3.4 10 keV

In this section the APD images and spectra corresponding to the 10 keV implantation zone (first plasma treatment) are shown.
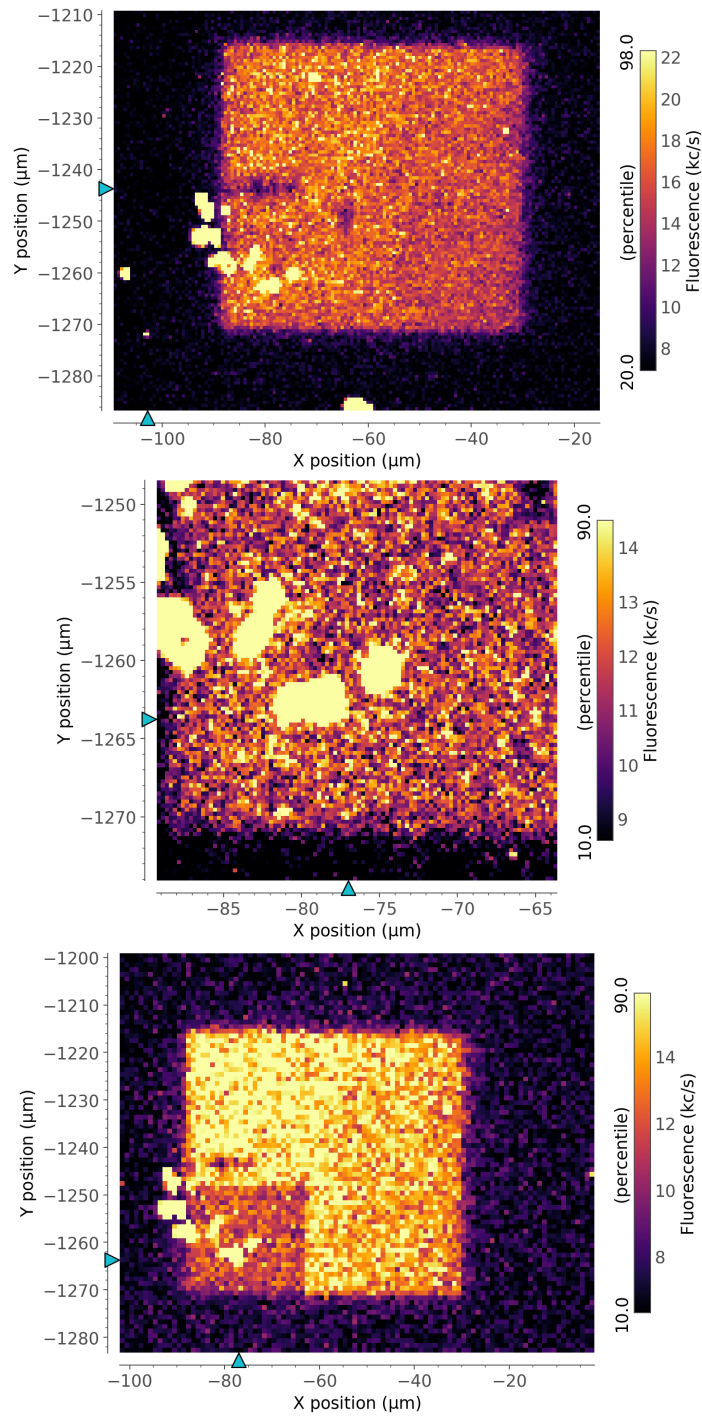

Figure 26: APD Image of 10 keV zone after 1st plasma treatment. Top: before bleach. Middle: inset bleach. Bottom: after bleach
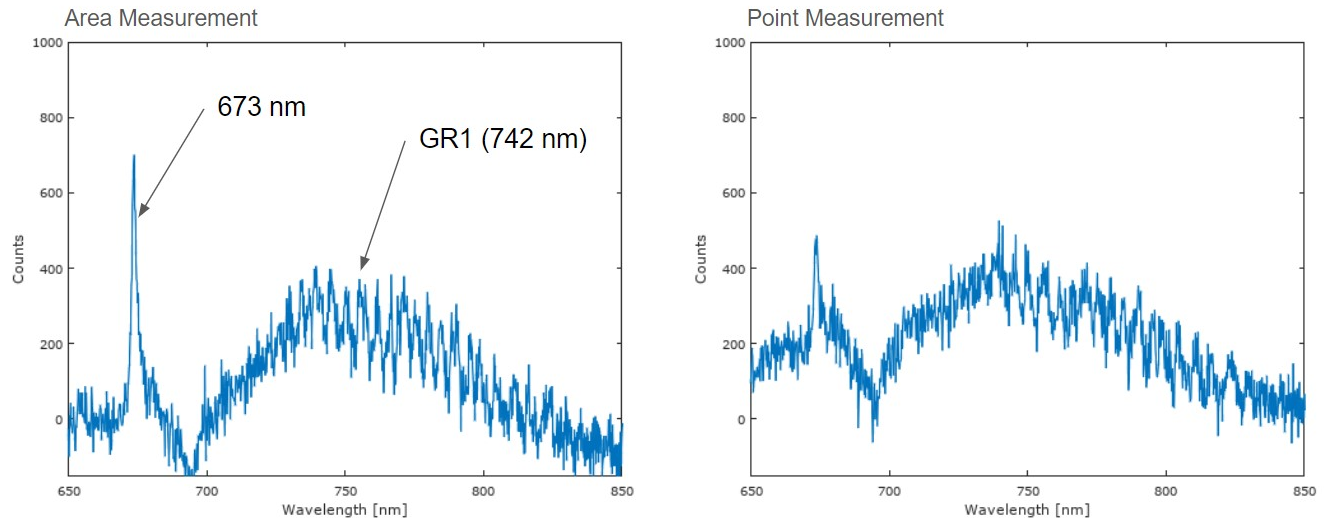
Figure 27: Spectra of the 10 keV zone after 1st plasma treatment. GR1 ZPL and an additional feature are indicated. Left: Area measurement. Right: Point measurement.

4.3.5 15 keV

In this section the APD images and spectra corresponding to the 15 keV implantation zone (first plasma treatment) are shown.
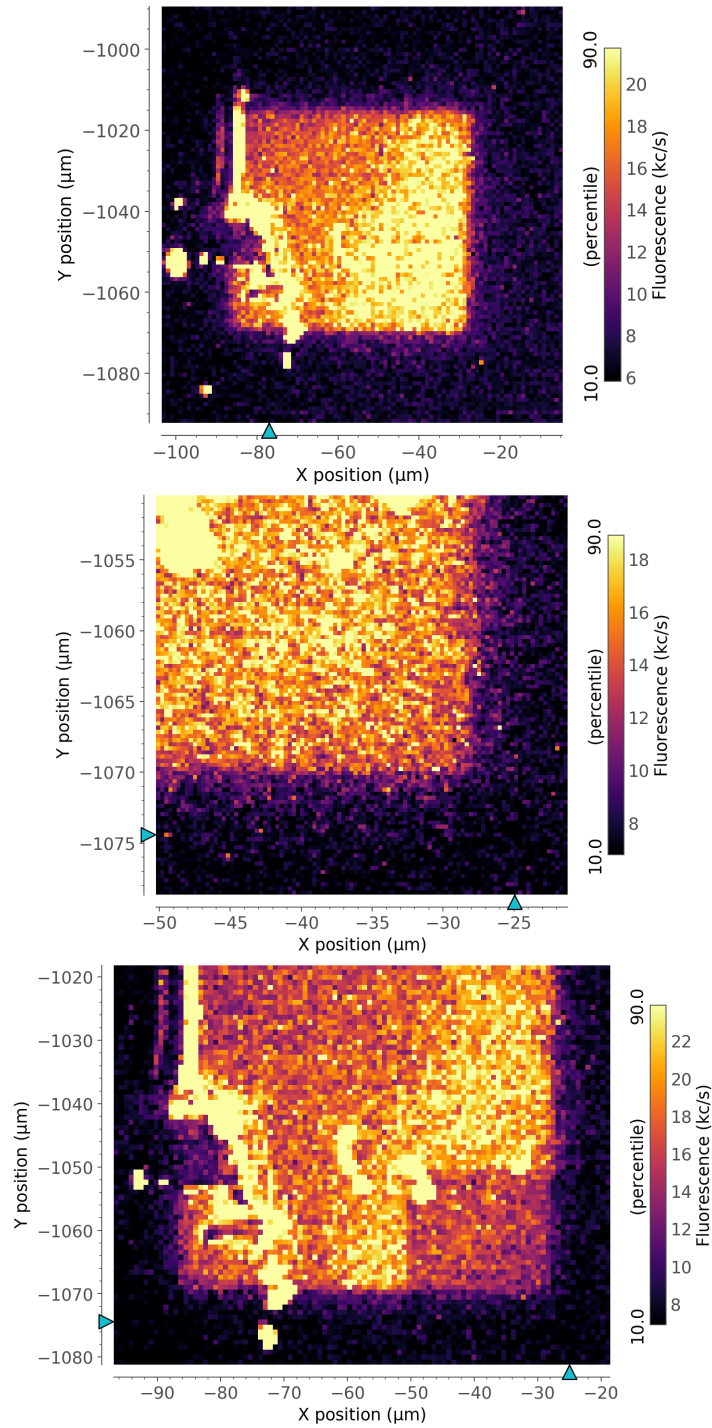

Figure 28: APD Image of 15 keV zone after 1st plasma treatment. Top: before bleach. Middle: inset bleach. Bottom: after bleach

Figure 29: Spectra of the 15 keV zone after 1st plasma treatment. GR1 ZPL and an additional feature are indicated. Left: Area measurement. Right: Point measurement.

4.3.6 20 keV

In this section the APD images and spectra corresponding to the 20 keV implantation zone (first plasma treatment) are shown.

Figure 30: APD Image of 20 keV zone after 1st plasma treatment. Top: before bleach. Middle: inset bleach. Bottom: after bleach
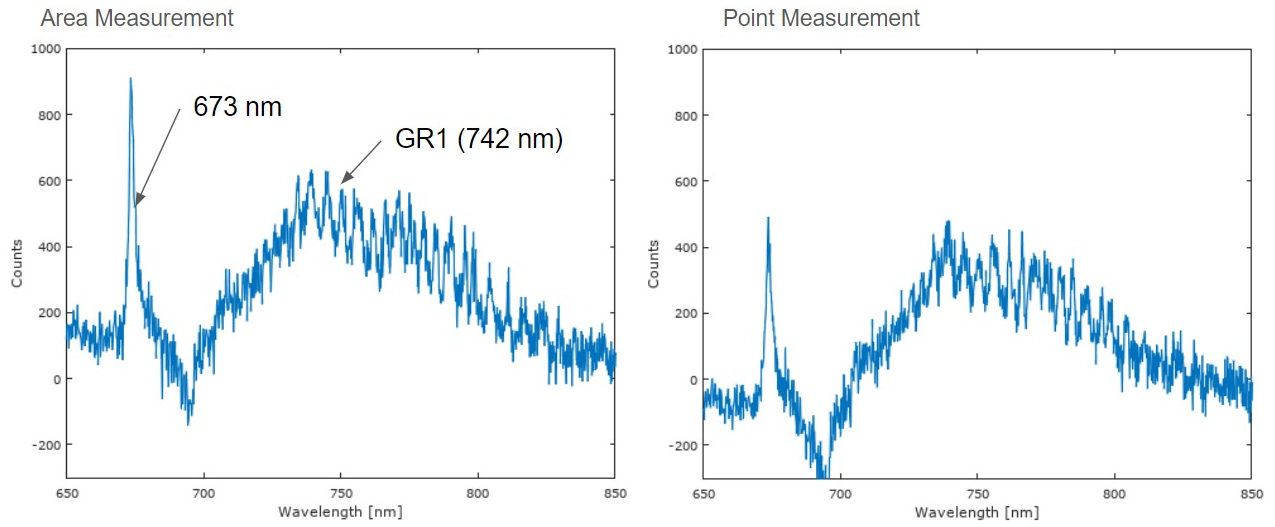
Figure 31: Spectra of the 20 keV zone after 1st plasma treatment. GR1 ZPL and an additional feature are indicated. Left: Area measurement. Right: Point measurement.

4.3.7 30 keV

In this section the APD images and spectra corresponding to the 30 keV implantation zone (first plasma treatment) are shown.
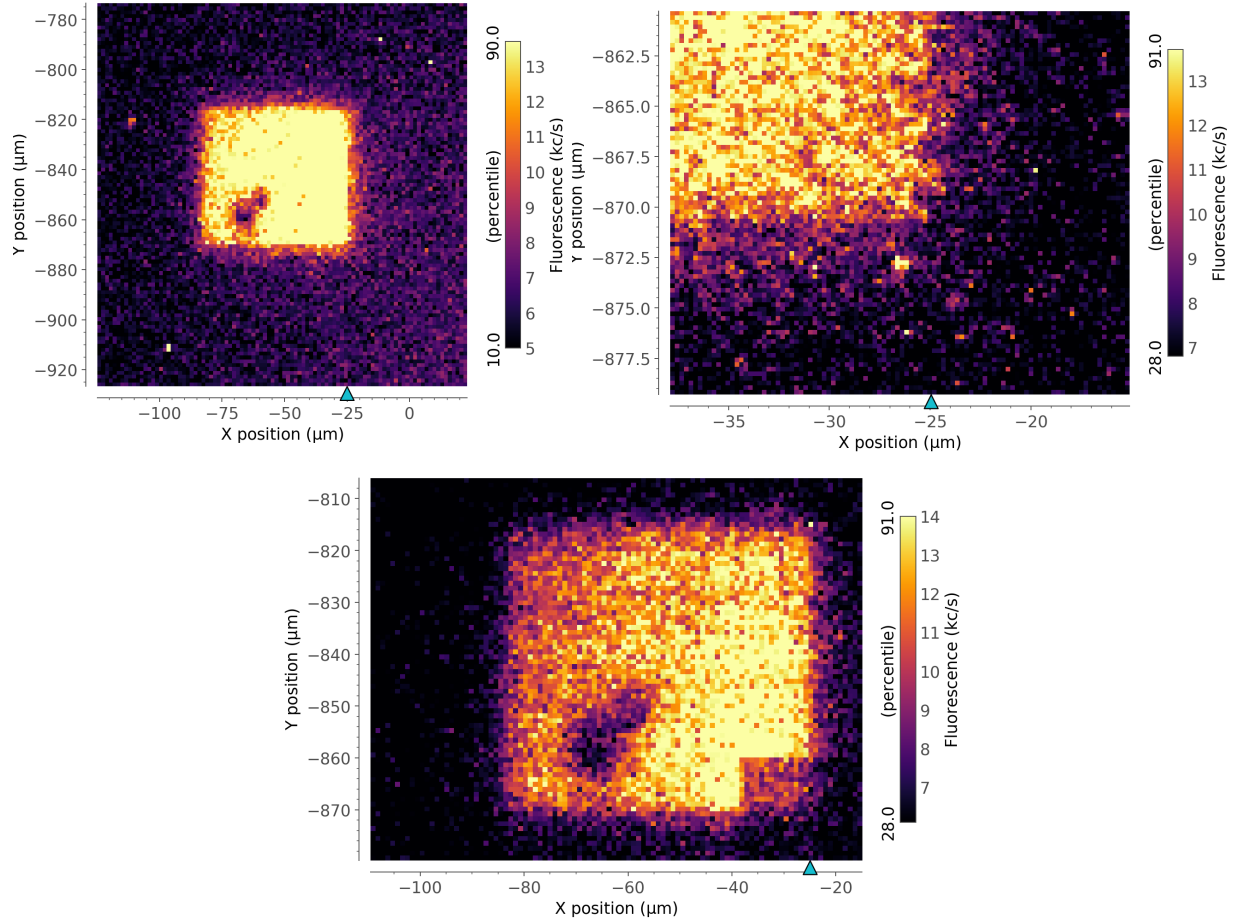

Figure 32: APD Image of 30 keV zone after 1st plasma treatment. Top left: before bleach. Top right: inset bleach. Bottom: after bleach
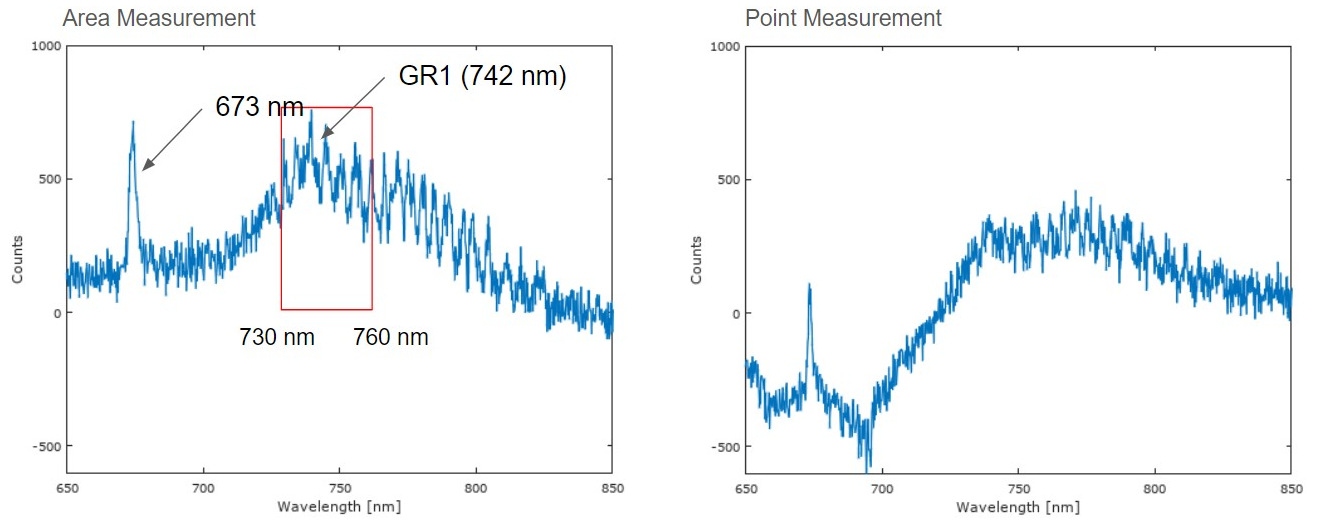
Figure 33: Spectra of the 30 keV zone after 1st plasma treatment. GR1 ZPL and an additional feature are indicated. Rectangle indicates where the signal is integrated. Left: Area measurement. Right: Point measurement.

4.3.8 GR1 Signal as a function of implantation energy

The area ($10\times10\ \mu$m) spectrum measurements seem to consistently acquire higher photon counts for GR1 features. As such, the approximate peaks of those measurements are plotted as a function of electron implantation energy in Fig. 34. Each data point is background subtracted and integrated from 730 nm to 760 nm from its respective data set. The overall tendency is an increase in the GR1 signal with increasing electron implantation energy.
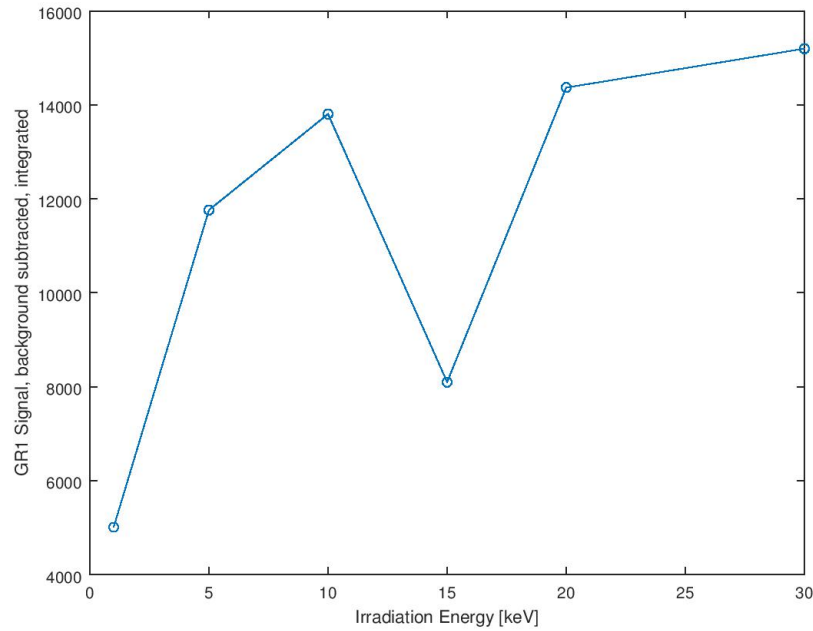

Figure 34: Plot of GR1 counts vs. electron implantation energy.

4.3.9 Additional feature at 673 nm

Through all spectrum measurements after plasma treatment, feature at 673 nm was clearly visible and often much stronger than the GR1 feature. There is a potential match in the literature at 670 nm, naturally occurring in some type IIa diamonds [2].

4.4 Plasma treatment 2, 20 minutes

4.4.1 Overview

For the second plasma treatment the settings of the plasma chamber were left largely the same except for the treatment duration of 20 minutes. The settings are 0,4 mbar pressure, room temperature and O_2 gas. The electron implantation pattern is the same as before and can be seen through fluorescence and with a diagram in Fig. 35. The spectra were acquired in the same manner as before, with 2 point measurements and 2 area measurements done inside and outside the respective implantation zone. The orange laser with $\lambda = 594$nm and a power of 390 μW was used. In the APD images the implantations where clearly visible, albeit with some dirt or residue gold particles left. Bleaching was clearly visible. As for the spectrum, GR1 signals were visible but relatively weaker. There are still strong peaks around 673 nm that were unexpected but already accounted for in the previous spectrum measurements.
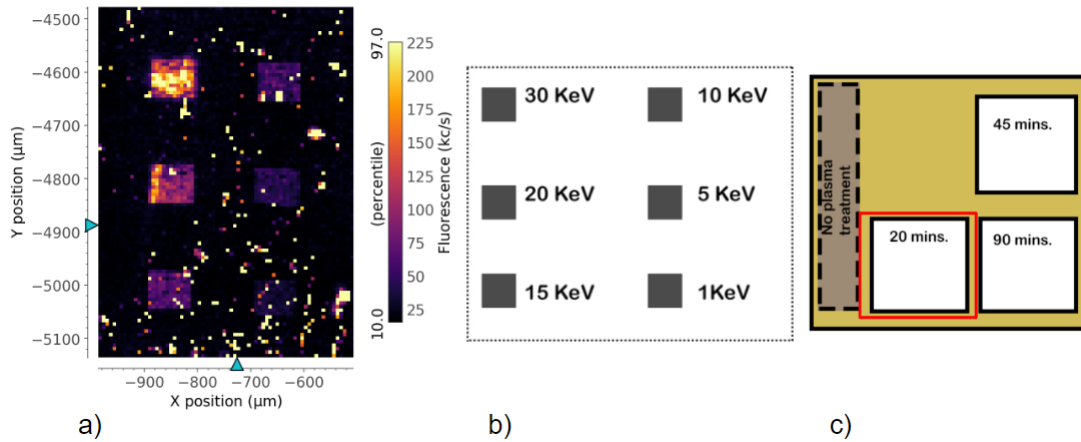

Figure 35: a): APD Image of all six implantation zones after 2nd plasma treatment. b): Diagram of all six implantation zones after 2nd plasma treatment. c): Relative location of the experimental step in the sample.

4.4.2   1 keV

In this section the APD images and spectra corresponding to the 1 keV implantation zone (2nd plasma treatment) are shown.
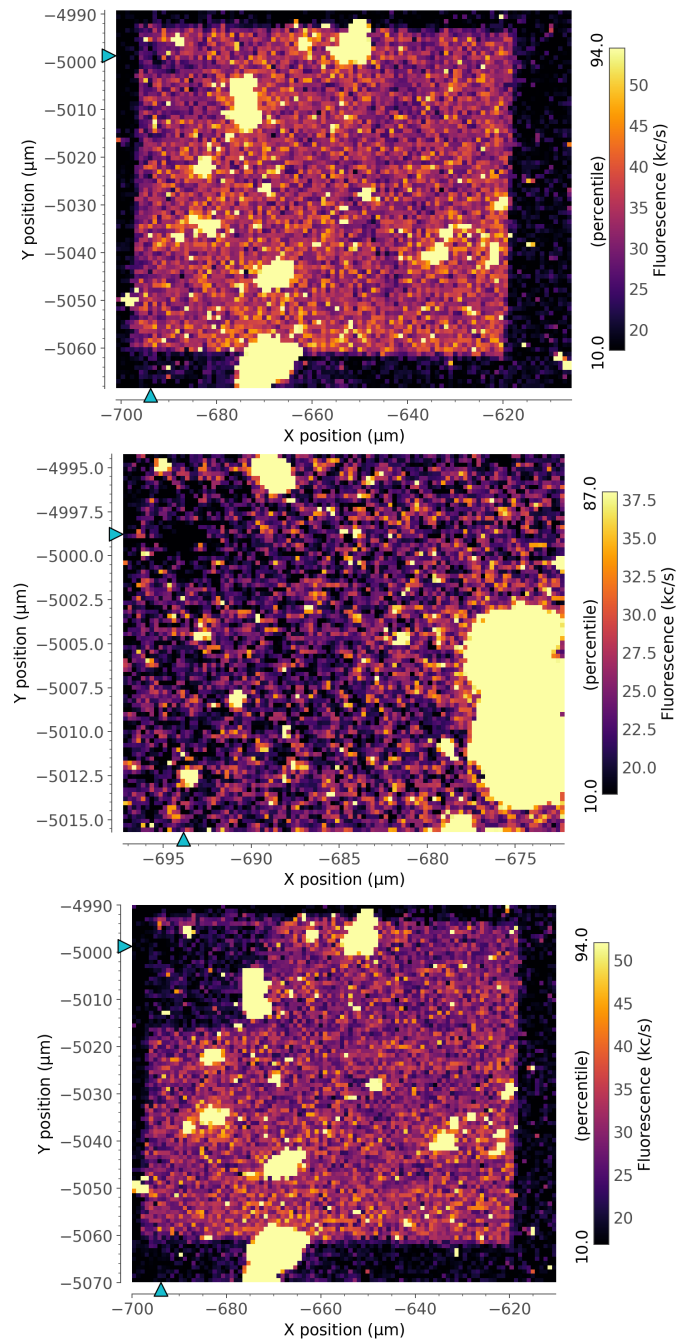

Figure 36: APD Image of 1 keV zone after 2nd plasma treatment. Top: before bleach. Middle: inset bleach. Bottom: after bleach
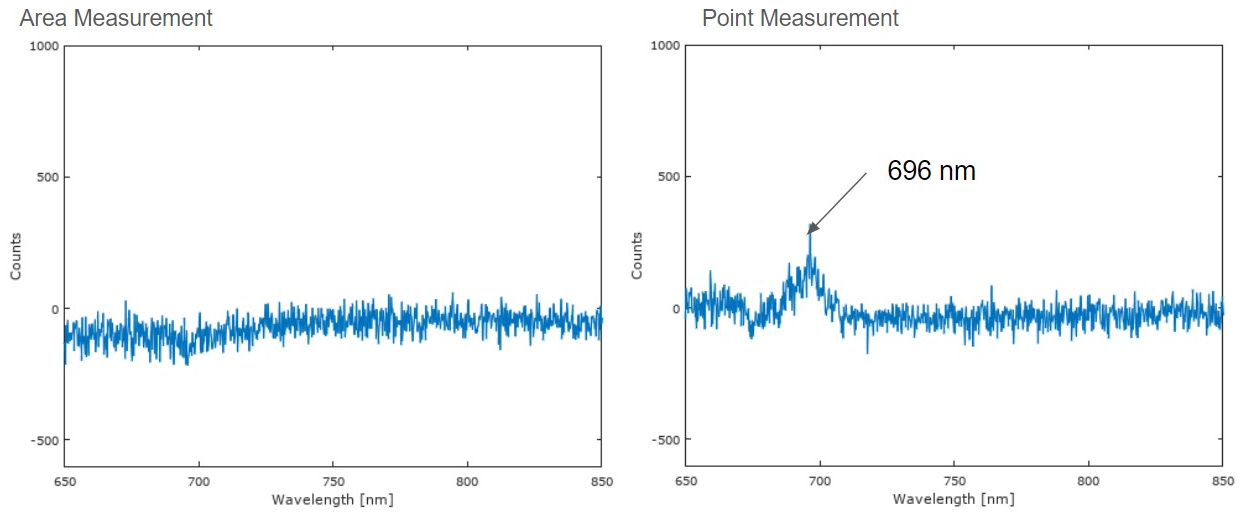
Figure 37: Spectra of the 1 keV zone after 2nd plasma treatment. A feature at 696 nm is indicated. Left: Area measurement. Right: Point measurement.

4.4.3   5 keV

In this section the APD images and spectra corresponding to the 5 keV implantation zone (2nd plasma treatment) are shown.
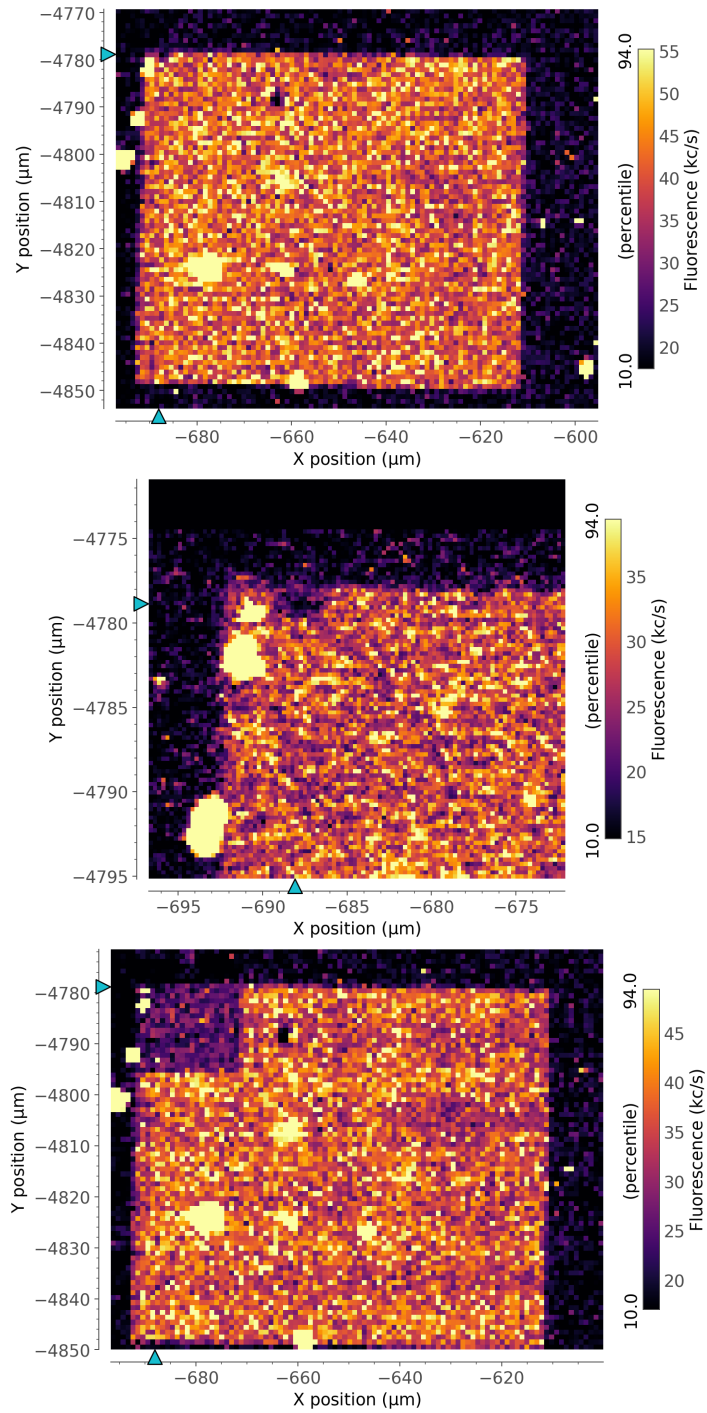

Figure 38: APD Image of 5 keV zone after 2nd plasma treatment. Top left: before bleach. Top right: inset bleach. Bottom: after bleach
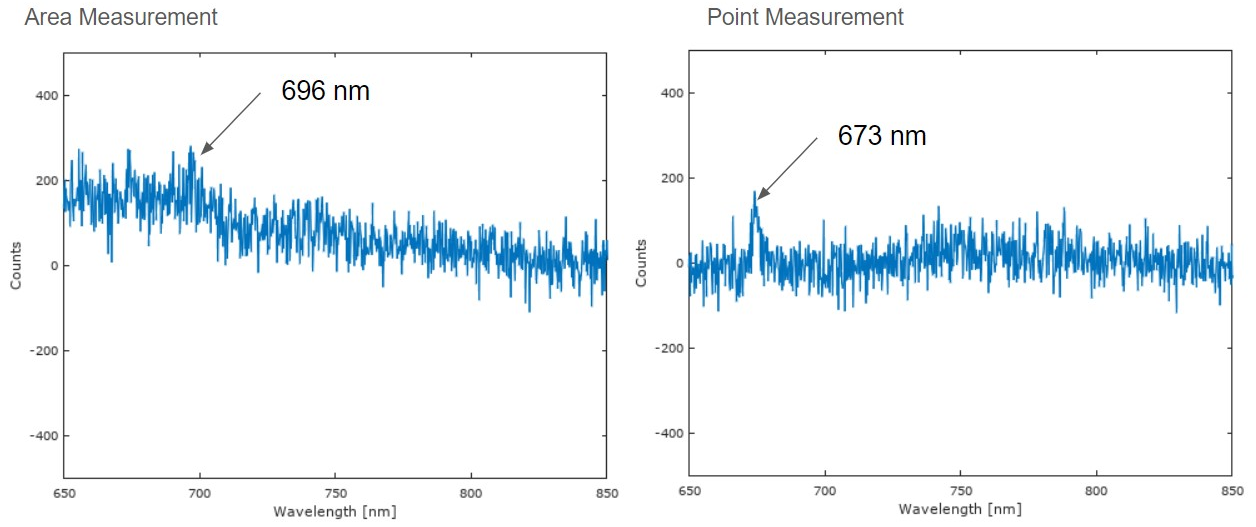
Figure 39: Spectra of the 5 keV zone after 2nd plasma treatment. A feature at 696 nm and 673 nm is indicated. Left: Area measurement. Right: Point measurement.

4.4.4 10 keV

In this section the APD images and spectra corresponding to the 10 keV implantation zone (2nd plasma treatment) are shown.
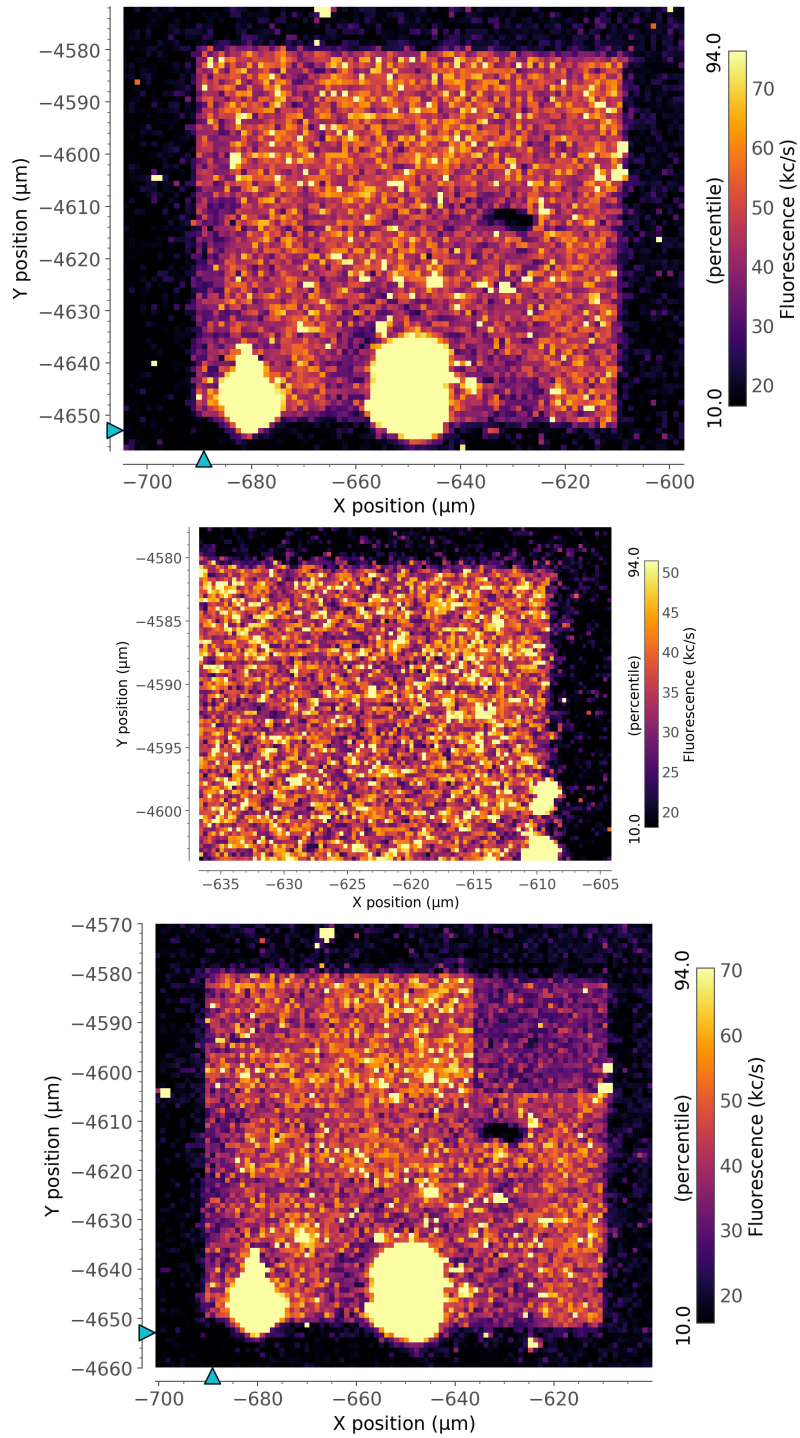

Figure 40: APD Image of 10 keV zone after 2nd plasma treatment. Top: before bleach. Middle: inset bleach. Bottom: after bleach

Figure 41: Spectra of the 10 keV zone after 2nd plasma treatment. GR1 ZPL and additional features are indicated. Left: Area measurement. Right: Point measurement.

4.4.5 15 keV

In this section the APD images and spectra corresponding to the 15 keV implantation zone (2nd plasma treatment) are shown.

Figure 42: APD Image of 15 keV zone after 2nd plasma treatment. Top: before bleach. Middle: inset bleach. Bottom: after bleach
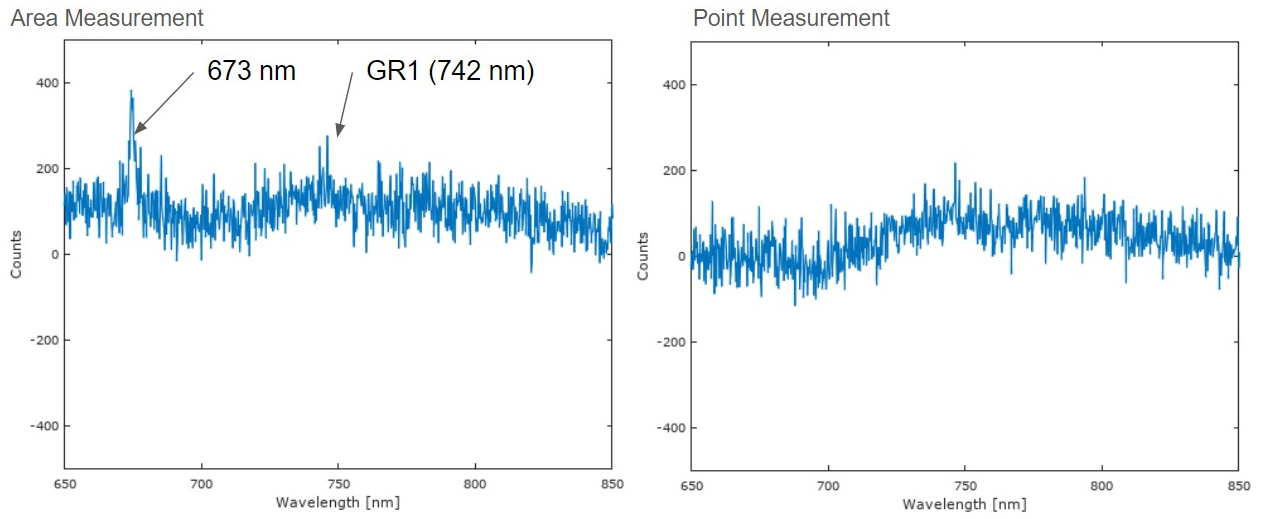
Figure 43: Spectra of the 15 keV zone after 2nd plasma treatment. GR1 ZPL and additional features are indicated. Left: Area measurement. Right: Point measurement.

4.4.6 20 keV

In this section the APD images and spectra corresponding to the 20 keV implantation zone (2nd plasma treatment) are shown.
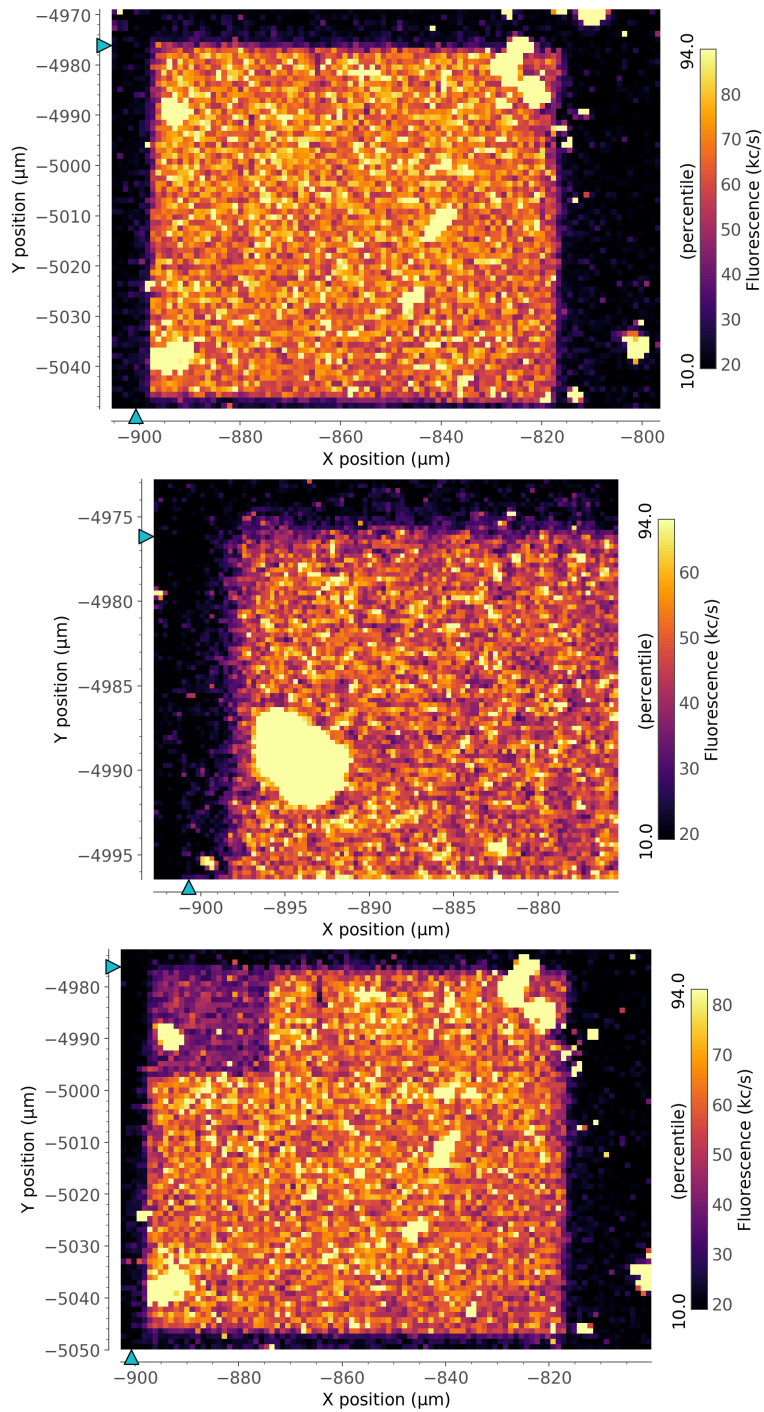

Figure 44: APD Image of 20 keV zone after 2nd plasma treatment. Top: before bleach. Middle: inset bleach. Bottom: after bleach
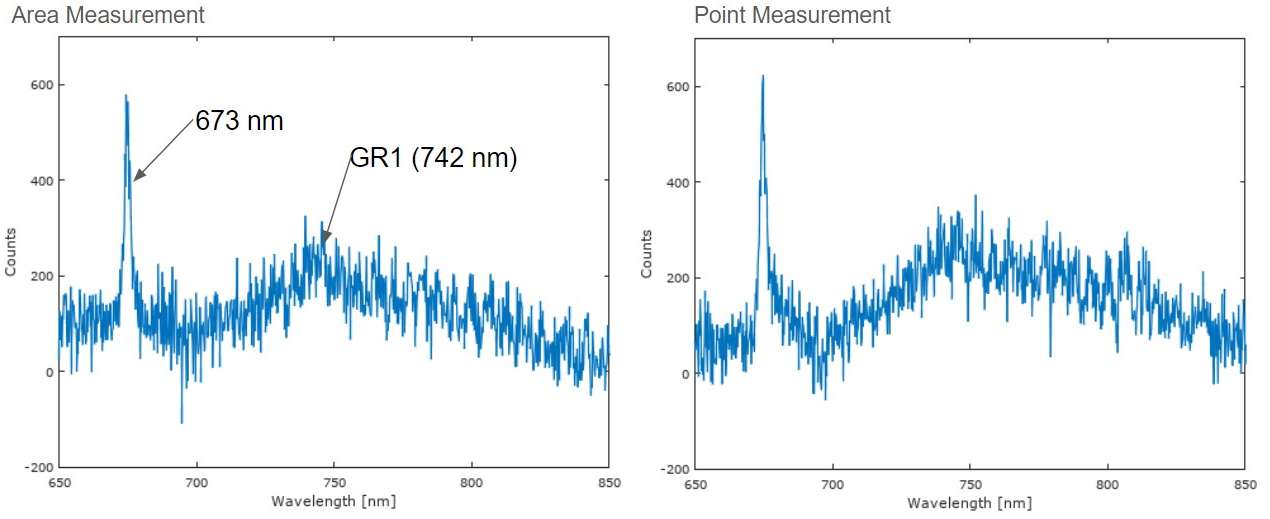
Figure 45: Spectra of the 20 keV zone after 2nd plasma treatment. GR1 ZPL and additional features are indicated. Left: Area measurement. Right: Point measurement.

4.4.7 30 keV

In this section the APD images and spectra corresponding to the 30 keV implantation zone (2nd plasma treatment) are shown.
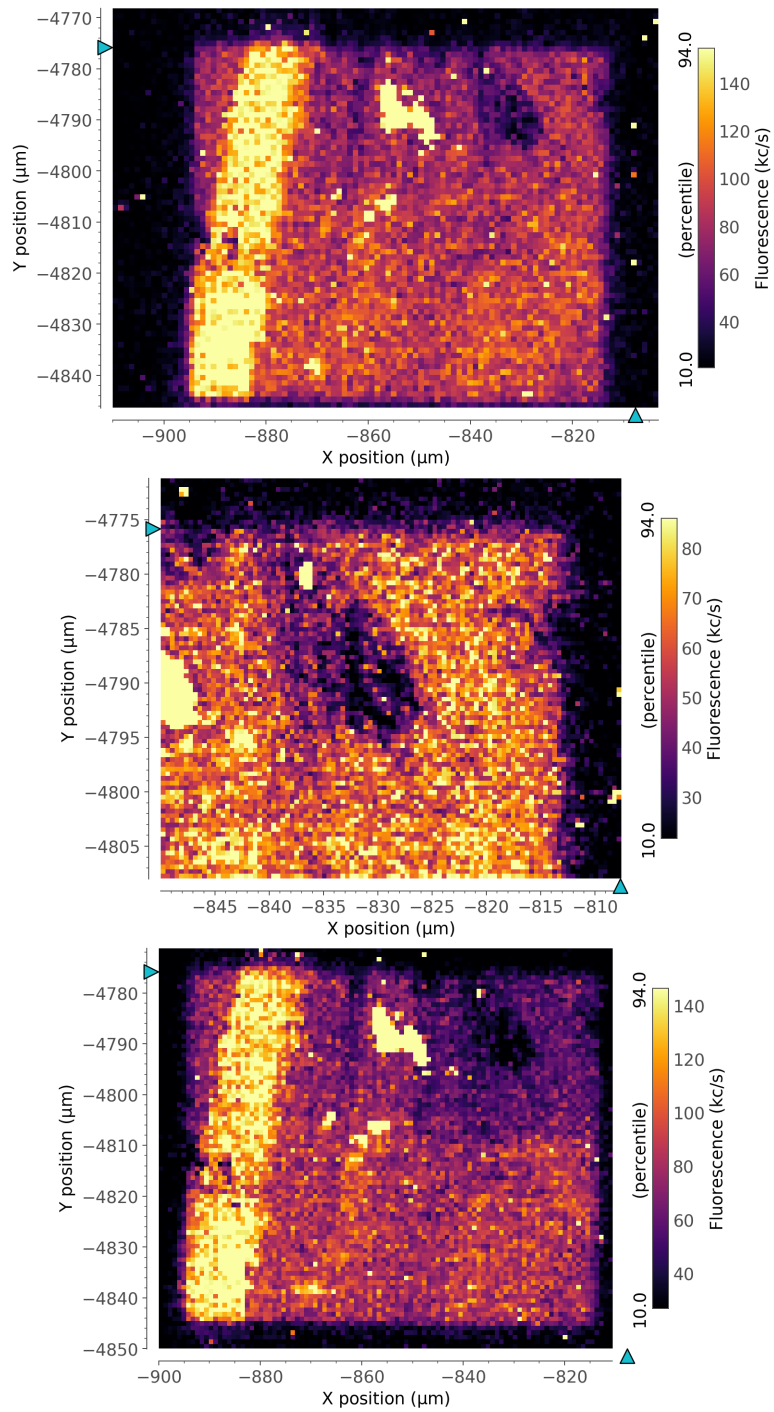

Figure 46: APD Image of 30 keV zone after 2nd plasma treatment. Top left: before bleach. Top right: inset bleach. Bottom: after bleach
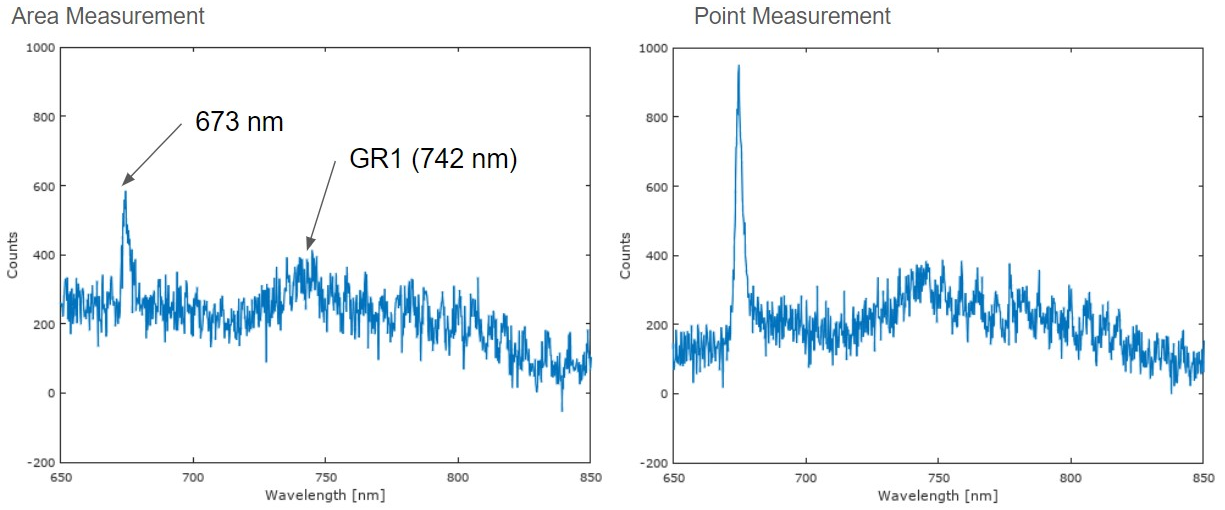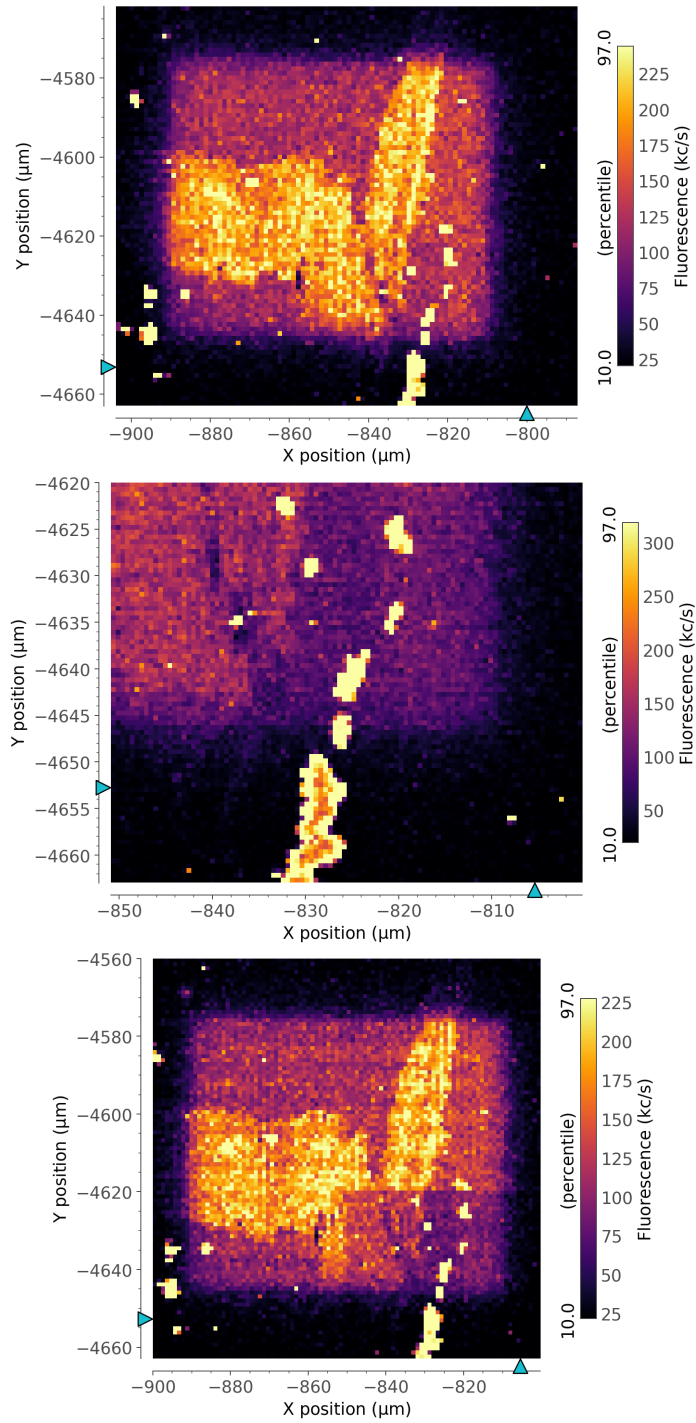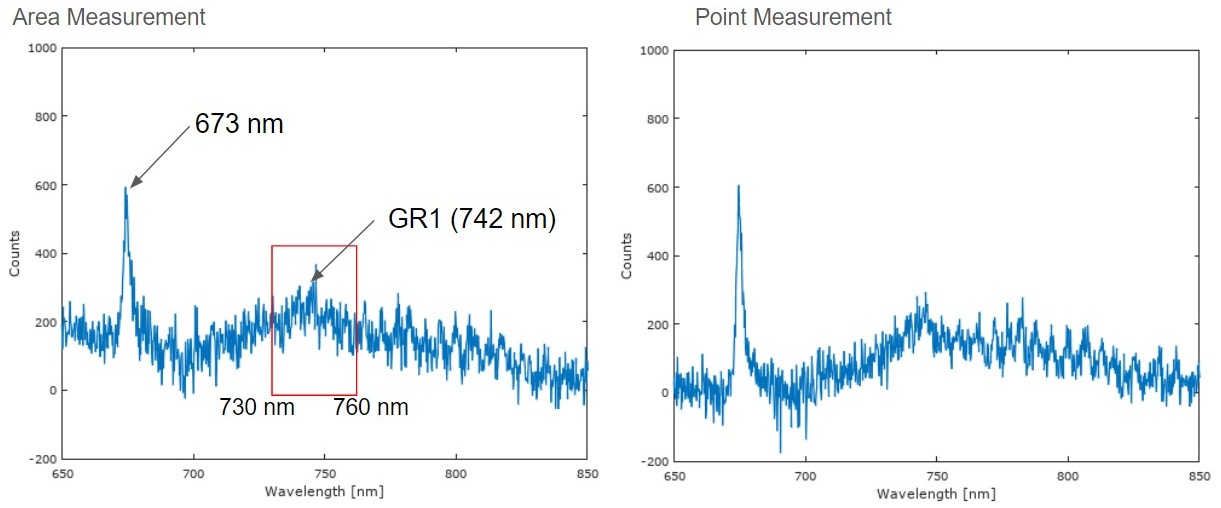
Figure 47: Spectra of the 30 keV zone after 2nd plasma treatment. GR1 ZPL and additional features are indicated. Integration limits are shown. Left: Area measurement. Right: Point measurement.

4.4.8 GR1 Signal as a function of implantation energy

The area (10×10 μm) spectrum measurements again seem to consistently acquire higher photon counts for GR1 features. As such, the approximate peaks of those measurements are plotted as a function of electron implantation energy in Fig. 48. In each data point the background was subtracted and the signal was integrated from 730 nm to 760 nm. The overall tendency is an increase in the GR1 signal with increasing electron implantation energy, although it is not a uniform increase.

Figure 48: Plot of GR1 counts vs. electron implantation energy.

4.5 GR1 Signal as a function of the plasma treatment

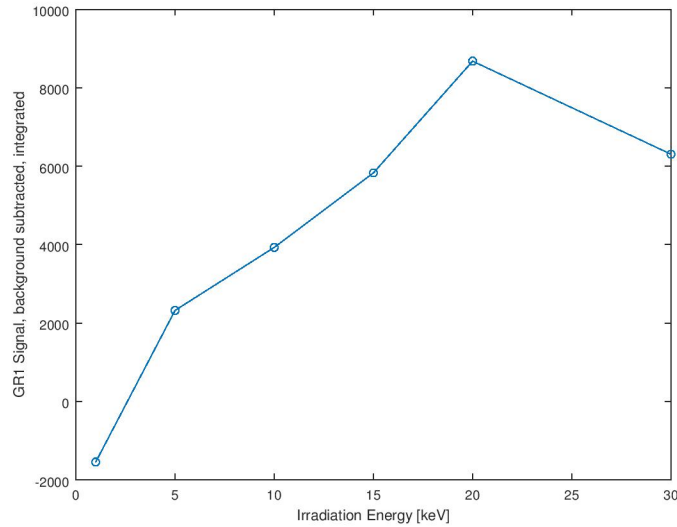It's clear that subjecting the sample to plasma treatment gave rise to GR1 features that were not there previously. The amount of time the sample spends in the plasma chamber, under the same conditions, could affect the intensity of this color center, although additionally plasma tests would be needed. In any case, it seems that surface effects from the plasma components are creating defects in the sample. It's suspected that the ionized O_2 is in the kinetic energy range necessary to create defects (100 eV - 500 eV) [3].

Fig. 49 is a plot of the GR1 counts vs. time spent in the plasma chamber. The main point is that the GR1 intensity seems to rise with the amount of time spent in the plasma chamber. Each curve corresponds to a given electron beam energy. For each curve the two points corresponding to 20 and 45 minutes in the plasma chamber are plotted. However, it may be debatable how comparable these points are, due to the fact that, in retrospect, there were differences in how the measurements were done. The parameters for the Confocal Scanning Laser Microscope are displayed, the difference being the laser power used. In retrospect the exact same power should have been used for more comparable data. However, the plasma chamber parameters, aside from the time, were identical (O_2 gas, 0.4 mbar pressure, room temperature). As before, all data points are taken from background-subtracted spectra, integrating the GR1 signal from 730 nm to 760 nm. In all cases the spectra were captured with a shutter time of 1 s with a total of 200 accumulations and a count frequency of 200 Hz.
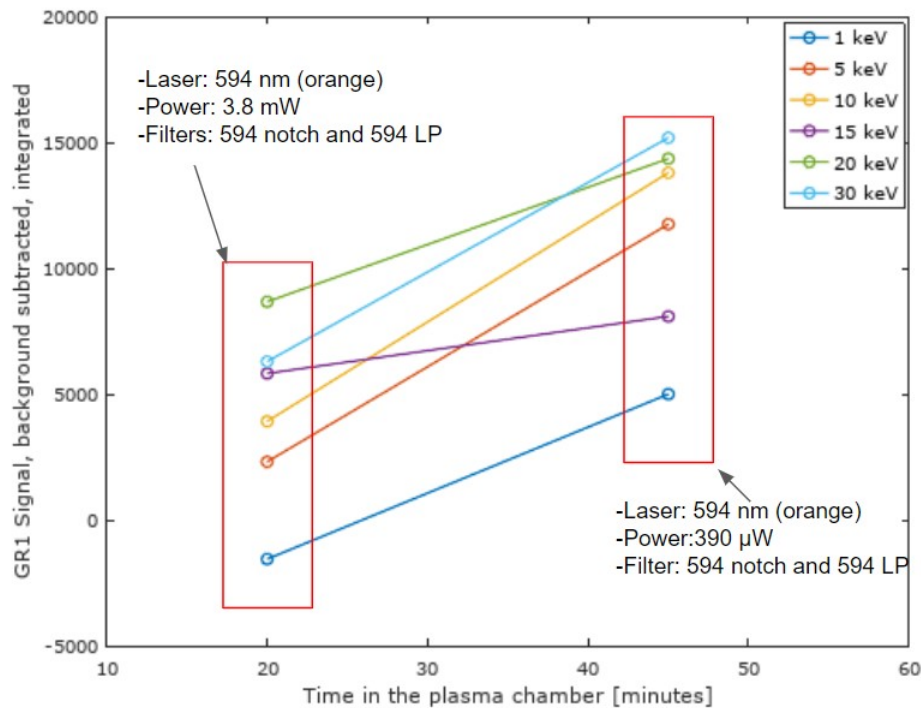

Figure 49: Plot of GR1 counts vs. plasma chamber time.

5 Conclusions and Outlook

The original objective was to quantify measurements and characteristics of GR1 color centers what were expected from the Electronic Grade Diamond from Element Six, using the Confocal Scanning Laser Microscope. No such color centers where found initially, necessitating the rest of the studies described previously. A heavy amount of Nitrogen impurities (extrinsic defects) and extreme bleaching on the surface of the sample (potentially due to dirt, despite previous chemical cleaning procedures) were found. The impurities were not expected in a sample of this category. The next step was to conduct experiments using the Pico plasma chamber. Beyond being a means to thoroughly clean up the sample, there was the opportunity to test whether plasma chamber treatment could create the GR1 defects. In order to test multiple plasma treatments, a layer of gold would be deposited using the Cressington Sputter Coater. This way, a small window could be scratched of for each plasma treatment, as a way of isolating the rest of the sample and having comparable results.

While the plasma treatment did diminish the short term transients and unstable signals, to the point that we were able to capture spectra, the bleaching still remained. More importantly the plasma chamber did create a number of defects on the sample, including but not limited to the sought-after GR1 color center. Notable features at 673 nm were detected and quite prominent. If anything, it shows that plasma treatment, while useful in cleaning up the sample, may cause potentially unwanted effects on the sample.

In addition, it was decided to test whether varying electron implantation energy would affect the spectral visibility of the GR1 color center. For this task multiple electron implantation zones where created with the Nova NanoLab 200 Electron microscope, and matching sets for each separate plasma treatment. GR1 photon counts were shown to increase with electron implantation energy, although not always so smoothly. In addition there seems so be an increase in GR1 color centers with increasing time in the plasma chamber, although the difference between a 20 minute treatment and a 45 minute treatment is not great in this regard. It suggests that the O_2 plasma might be creating neutral charge state vacancies in the diamond lattice through impacts with sufficient kinetic energy, displacing certain carbon atoms. The technique of testing the same sample multiple times while shielding it with a removable layer of gold seems to be effective.

As a result this may provide an alternative method to create such defects when the advantages of GR1 color centers for quantum systems are desired. On the other hand it may be a cause for concern when such effects are not desired. However, additional testing with the plasma chamber would be required to ascertain this and quantify it further, under additional circumstances. Testing larger time ranges and perhaps different gases would be a potential area of investigation. In addition, different samples might yield different results. In any case it seems wise to verify any spectral changes in samples of this type when using plasma treatment.

6 Bibliography

[1] Schwartz, J., et al. Effects of Low-Energy Electron Irradiation on Formation of Nitrogenvacancy Centers in Single-Crystal Diamond. New Journal of Physics 14.4 (2012): 043024.

[2] A. Zaitsev, *Optical Properties of Diamond: A Data Handbook*. Springer, 2001.

[3] R. Hippler, S. Pfau, et al. *Low temperature plasma physics: fundamental aspects and applications*. Wiley, 2001.

[4] C. Bräutigam, Untersuchung zur Auswirkung einer niederfrequenten Sauerstoffplasmabehandlung auf oberflächennahe NV-Zentren im Diamanten, Bachelors thesis, Universität Leipzig - Fakultät für Physik und Geowissenschaften, 2017.

[5] R. Staacke, Magnetometrie nicht klassischer Leitungsmechanismen in amorphen Halbleitern mit Hilfe einzelner NV-Zentren, Master's thesis, Universität Leipzig - Fakultät für Physik und Geowissenschaften, 2015.

[6] A. Kuehne, "Photolumineszenzspektroskopische Bewertung von Passivierungseffekten durch Wasserstoff auf NV-Zentren in Diamant", Master's thesis, Universität Leipzig - Fakultät für Physik und Geowissenschaften, 2017.

[7] Diener Electronic GmbH Co. KG (Hrsg.): *Plasma-Technik*. Diener Electronic GmbH Co. KG,2016. https://www.plasma.com/en/produkte/plasmaanlagen/niederdruckplasma-anlagen/pico/

[8] Element Six Technologies, De Beers Group (Hrsg.): *The Element Six CVD Diamond Handbook*. Element Six Technologies De Beers Group, 2016

[9] I. Kiflawi, A. Collins, et al. "Electron irradiation and the formation of vacancy-interstitial pairs in diamond" Journal of Physics: Condensed Matter 19 (2007): 046216.

[10] Sébastien Pezzagna et al 2011 New J. Phys. 13 035024

[11] Gemological Institute of America Inc.: *Optical Defects in Diamond: A Quick Reference Chart*. Gemological Institute of America Inc., 2019. https://www.gia.edu/gems-gemology/summer-2013-shigley-optical-defects-diamond

[12] I. Kiflawi, A. Collins, et al. "Optical absorption and luminescence in diamond" Journal of Physics: Rep. Prog. Phys., Vol. 42, (1979).

[13] R. D'Agostino, P. Favia, et al. *Advanced plasma technology*. Wiley, 2008.

[14] Perkin Elmer (Hrsg.): *Single Photon Counting Modules - SPCM*. Perkin Elmer. https://www.perkinelmer.com/PDFS/downloads/dts_photodiodemodulesreceiverforanalyticalmolecularapplications.pdf

7 Appendix

7.1 Table of Properties of Element Six Electronic Grade Diamond

PROPERTIES	SINGLE CRYSTAL	POLYCRYSTALLINE	COMMENTS
ELECTRONIC			
Hole mobility ($cm^2V^{-1}s^{-1}$)	>2000	1000	
Electron mobility ($cm^2V^{-1}s^{-1}$)	>2000	1800	
Carrier lifetime (ns)	~2000	~ 1 - 10	
Charge collection distance	*Typically >475μm	†Typically >180μm	*At 0.5 V μm^{-1} applied field, for 500 μm plate † At 1V um^{-1} applied field, for 500 μm plate
Charge Collection Efficiency	Typically >95%	Typically >36%	for 500 μm plate
Bandgap (eV)	5.47	5.47	
Electron saturation velocity (cms^{-1}) x 10^7	2	2	
Radiation Hardness cm^{-2} 24 GeV protons		>10^{15}	With <25% signal drop
Breakdown Voltage (MV cm^{-1})	1 - 2		Experimental value. Threshold current 10 μA 4 x 4 mm x 20 μm contact area 0.71 mm^2
IMPURITIES			
$[N]^0_s$ (ppb)	<5 (typically 0.1 -1)	<50	Measured by EPR
[B] (ppb)	<1	<1	Measured by SIMS
THERMAL PROPERTIES			
Thermal conductivity (W m^{-1}K^{-1})	>2000	> 1900	
Expansion Coefficient (ppm K^{-1}) at 300 K	1.0 ± 0.1	1.0 ± 0.1	
Expansion Coefficient (ppm K^{-1}) at 1000 K	4.4 ± 0.1	4.4 ± 0.1	
DIMENSIONS			
Standard Sizes (mm)	2x2, 3x3, 4.5x4.5	5.5, 10x10, 20x20	Tolerance ± 0.05 mm Polycrystalline available up to Ø110mm
Standard thickness (mm)	0.3 & 0.5	0.3 & 0.5	Tolerance ± 0.05 mm
Laser kerf	3°	3°	
Edge Features (mm)	< 0.2	< 0.2	
Crystallographic Orientation (face / edge)	[100] ± 3° <110>		
PROCESSED			
Surface finish side 1 Ra (nm)	<0.5	Ra <20	Single crystal polished on [100] face
Surface finish side 2 Ra (nm)	<0.5	Ra <20	Single crystal polished on [100] face

Figure 50: Table of Properties of Element Six Electronic Grade Diamond [8].

8 Acknowledgments

9 Statement of authorship

I hereby certify that this bachelor thesis has been composed by myself and describes my own work, unless otherwise acknowledged in the test. All references and verbatim extracts have been quoted and all sources of information have been specifically acknowledged. It has not been accepted in any previous application for a degree.

Leipzig, 28. Juli 2019   Marvin Mellado Muñoz